Liver Fibrosis, Fat, and Iron Evaluation with MRI and Fibrosis and Fat Evaluation with US: A Practical Guide for Radiologists

Flavius F. Guglielmo, MD • Richard G. Barr, MD, PhD • Takeshi Yokoo, MD, PhD • Giovanna Ferraioli, MD • James T. Lee, MD • Jonathan R. Dillman, MD, MSc • Jeanne M. Horowitz, MD • Kartik S. Jhaveri, MD • Frank H. Miller, MD • Roshan Y. Modi, MD, MBA, MHA • Amirkasra Mojtahed, MD Michael A. Ohliger, MD, PhD • Ali Pirasteh, MD • Scott B. Reeder, MD, PhD • Krishna Shanbhogue, MD • Alvin C. Silva, MD • Elainea N. Smith, MD Venkateswar R. Surabhi, MD • Bachir Taouli, MD, MHA • Christopher L. Welle, MD • Benjamin M. Yeh, MD • Sudhakar K. Venkatesh, MD

Author affiliations, funding, and conflicts of interest are listed at the end of this article.
See the invited commentary by Ronot in this issue.

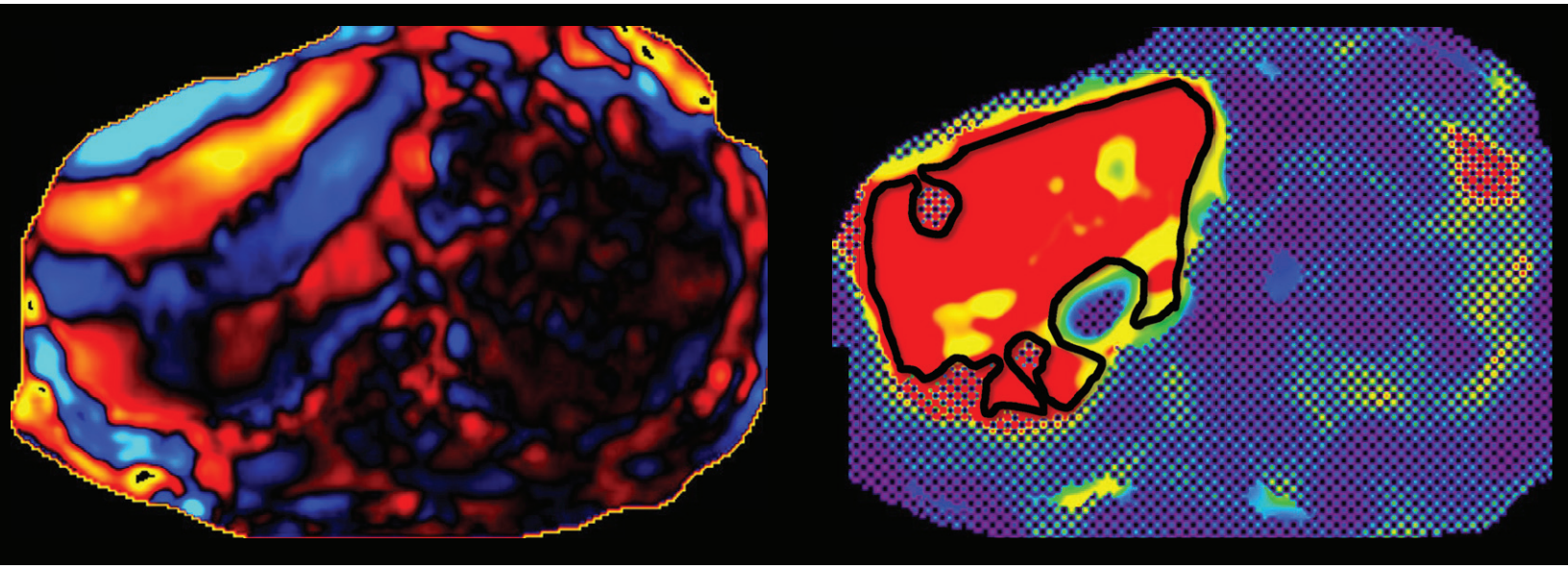

Quantitative imaging biomarkers of liver disease measured by using MRI and US are emerging as important clinical tools in the management of patients with chronic liver disease (CLD). Because of their high accuracy and noninvasive nature, in many cases, these techniques have replaced liver biopsy for the diagnosis, quantitative staging, and treatment monitoring of patients with CLD. The most commonly evaluated imaging biomarkers are surrogates for liver fibrosis, fat, and iron. MR elastography is now routinely performed to evaluate for liver fibrosis and typically combined with MRI-based liver fat and iron quantification to exclude or grade hepatic steatosis and iron overload, respectively. US elastography is also widely performed to evaluate for liver fibrosis and has the advantage of lower equipment cost and greater availability compared with those of MRI. Emerging US fat quantification methods can be performed along with US elastography. The author group, consisting of members of the Society of Abdominal Radiology (SAR) Liver Fibrosis Disease-Focused Panel (DFP), the SAR Hepatic Iron Overload DFP, and the European Society of Radiology, review the basics of liver fibrosis, fat, and iron quantification with MRI and liver fibrosis and fat quantification with US. The authors cover technical requirements, typical case display, quality control and proper measurement technique and case interpretation guidelines, pitfalls, and confounding factors. The authors aim to provide a practical guide for radiologists interpreting these examinations.

RG GASTROINTESTINAL IMAGING

Invited Commentary

Supplemental Material

Quiz questions for this article are available in the supplemental material.

RadioGraphics 2023; 43(6):e220181
https://doi.org/10.1148/rg.220181

Content Codes: GI, MR, US

Abbreviations: ARFI = acoustic radiation force impulse, cALCD = compensated advanced CLD, CLD = chronic liver disease, CSE = chemical shift–encoded, IQR/M = interquartile range–to-median ratio, LIC = liver iron concentration, LS = liver stiffness, LSM = LS measurement, mSGRE = multiecho spoiled gradient recalled echo, MRE = MR elastography, PDFF = proton density fat fraction, ROI = region of interest, SWE = shear wave elastography, TE = echo time

TEACHING POINTS

- A good-quality MR elastography (MRE) examination has the following features: signal void in the abdominal wall, sections obtained through the mid liver, good shear wave propagation in the liver, and a large region of liver parenchyma available for liver stiff measurement (LSM).
- Fat-water swaps can affect only a portion of a single image or the entire series. Regions of interest (ROIs) should not be placed in swapped areas as the PDFF values are incorrect.
- In patients with severe or extreme iron overload, the signal may decay too fast for the mSGRE acquisition to measure the liver signal intensity adequately before it decays to noise. When this occurs, the R2* estimation becomes computationally unstable, resulting in imprecise estimates and a speckled "snowstorm" appearance on the R2* map.
- It should be noted that with US, LSM is reported as the Young modulus in kilopascals, while with MRE, LSM is reported as the magnitude of the complex shear modulus, also in kilopascals. US measurements in kilopascals are approximately three times the kilopascals reported with MRE when performed at the same frequency. However, since the Young modulus and shear modulus measure two different entities, conversion of LSM measurements obtained with US SWE and MRE should generally be avoided.
- New quantitative US methods to assess liver fat content have recently been developed. These techniques analyze the radiofrequency echoes returning to the transducer and calculate parameters that can be used to quantify liver fat content. They include attenuation coefficient, backscatter coefficient, and speed of sound, as well as combinations of these.

Introduction

Chronic liver disease (CLD) is a significant cause of mortality, morbidity, and health care expenditure and is responsible for more than 44 000 deaths each year in the United States and 2 million deaths worldwide (1). The most common causes of CLD are nonalcoholic fatty liver disease (NAFLD), chronic viral hepatitis B and C infections, and alcohol-related liver disease. The epidemiology of CLD has shifted over the last decade as a result of effective antiviral regimens and increased prevalence of NAFLD resulting from the global obesity epidemic (1,2).

For patients with CLD, an emerging patient management clinical tool is quantitative imaging biomarkers of liver disease. Currently, commercially available liver imaging biomarkers include MRI measurement of fibrosis, fat, and iron concentration, and US measurement of fibrosis and fat. US is not used for iron quantification. Historically, diagnosis and staging of liver fibrosis, fat, and iron has relied on liver biopsy. However, liver biopsy has limitations including sampling error, cost, invasiveness, morbidity, pathologist interreader reporting variability, and low patient acceptance (3). For the same reasons, repeat biopsy to assess for treatment response is undesirable. Biopsies sample only a small portion of the liver, which may not accurately reflect overall liver involvement when there is heterogeneous distribution in the liver. As MRI and US biomarker technologies have become more available, they have successfully replaced liver biopsy in many patient care settings, owing to availability, repeatability, and improved patient acceptance.

For fibrosis detection and staging, MR elastography (MRE) is now routinely performed in many radiology practices (4). In most centers, MRE is combined with MRI-based fat and iron quantification to provide a comprehensive liver biomarker panel (5). Dedicated liver US shear wave elastography (SWE) and fat quantification can be easily added to a standard abdominal US examination. The greater availability and lower equipment cost of US compared with MRI makes US more convenient in routine clinical care.

In this article, our author group, which consists of members of the Society of Abdominal Radiology (SAR) Liver Fibrosis Disease-Focused Panel (DFP), the SAR Hepatic Iron Overload DFP, and the European Society of Radiology, reviews the basics of quantifying liver fibrosis, fat, and iron concentration with MRI and quantifying liver fibrosis and fat with US. This includes a review of technical requirements, typical case display, quality control, measurement technique, and case interpretation guidelines, pitfalls, and confounding factors. Our goal is to provide a practical guide for radiologists interpreting these examinations.

MR Elastography

Overview

MRE can be performed by adding hardware and software to existing or new 1.5-T and 3-T MRI scanners (6). The clinical liver MRE setup consists of an active driver placed outside the MRI scanner room connected to a passive driver via a plastic tube through a waveguide in the wall (Fig 1). The passive driver is placed over the right hepatic lobe by using the midclavicular line and xiphisternum as landmarks and held in place with an elastic strap. The passive driver is securely fastened on the abdominal wall to ensure that vibrations are transmitted into the abdominal wall and liver (6,7). In general, we recommend that all acquisitions are performed with the patient at end expiration, which ensures reproducible positioning of the diaphragm and liver (Fig 2) (8). The passive driver delivers acoustic vibrations produced by the active driver and creates propagating shear waves that are imaged with the MRE sequence. The raw data (ie, magnitude and phase images) are immediately available for review on the scanner workstation. The wave information contained in the raw data is then processed by an automatic inversion algorithm that produces an elastogram in gray scale and/or color scale. Additional images may be produced depending on the vendor including gray-scale and color-wave images and gray-scale and color elastograms with and without a confidence map (Fig 3; Appendix S1).

MRE Quality Control

Each MRE sequence performed must be reviewed for quality to ensure that any liver stiffness measurement (LSM) obtained will be valid and for troubleshooting. All liver MREs should be obtained at a fixed 60-Hz frequency, which is standardized

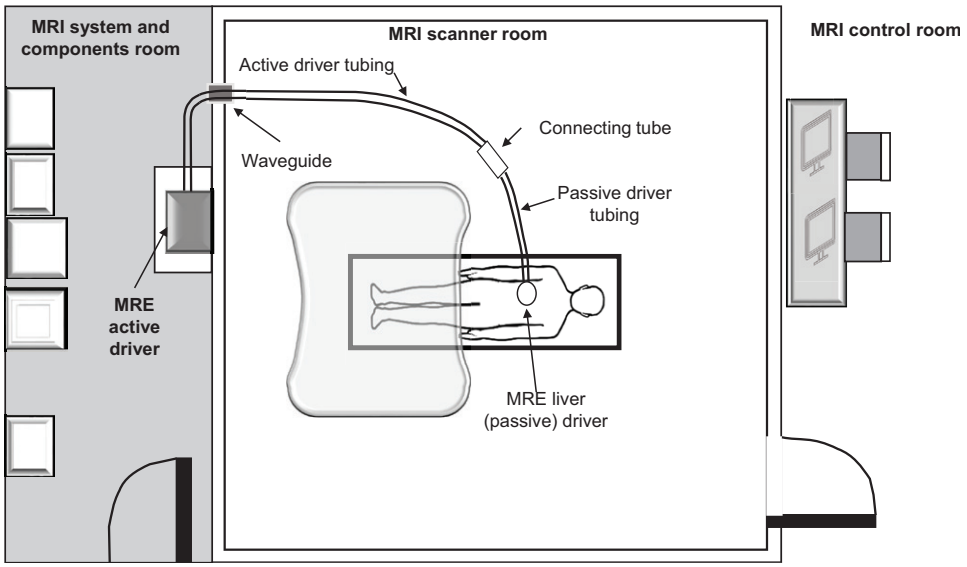

Figure 1. Diagram shows the typical liver MRE setup. The MRE active driver (ferromagnetic) is located outside of the MRI scanner room, typically in the MRI system and components room. The pneumatic tubing from the active driver passes through the waveguide in the wall between the scanner room and the components room. The tube is then connected to the passive driver tubing via the connecting tube, ensuring continuity of the active and passive drivers at either end. On this illustration, the patient is scanned in the feet-first supine position, although this can be changed to the headfirst supine position depending on the MRI system configuration. The passive driver is placed over the liver by using the midclavicular line and xiphisternum as landmarks and then held in close contact with an elastic wrap.

MRI Scanner Parameters	1.5T*	3T*	Patient Preparation
Pulse sequence	2D gradient echo	2D spin echo - EPI	4–6 hour fast
Orientation	Transverse	Transverse	
TR	50 msec	1000 msec	**Patient Position**
TE	Min TE (~18.2 msec)	MinFULL (~55.4 msec)	Supine
Section thickness	10 mm	8 mm	
Section gap	0 mm	2 mm	**Passive Driver Placement**
Phase encoding direction	Right to Left	Right to Left	RUQ; centered over liver
FOV read (patient specific)	420 mm	420 mm	
Number of sections	4	4–9	**Section Placement**
Averages	1	1	Largest cross section of liver
Flip angle	25°	90°	
Acquisition matrix	256 x 64	80 x 80	**Breath Hold**
Typical scan time	55 sec (11–15 sec/section)	16 sec	Passive driver placed and all sequences obtained in end-expiration, which is more reproducible
MRE driver frequency	60 Hz	60 Hz	
MEG frequency	60 Hz	60 Hz	
MEG direction	(Z-direction)	(Z-direction)	**Active Driver**
Amplitude (BMI 19–29)†	50%	50%	Located outside of imaging room
Respiratory control	Breath hold	Breath hold	
Bandwidth	31.25 kHz	250 kHz	

Figure 2. Chart shows a sample MRE protocol. *Detailed protocols from multiple MRI vendors and MRI systems are available in the Radiological Society of North America (RSNA) Quantitative Imaging Biomarkers Alliance (QIBA) Profile (8). †For a body mass index *(BMI)* less than 19, use 30% amplitude; for BMI greater than 29, use 70% amplitude. *EPI* = echo-planar imaging, *FOV* = field of view, *MEG* = motion-encoded gradient, *Min* = minimum, *RUQ* = right upper quadrant, *TE* = echo time, *TR* = repetition time, *2D* = two dimensional.

across all scanners and field strengths (Fig 2). A good-quality MRE examination has the following features: signal void in the abdominal wall, sections obtained through the mid liver, good shear wave propagation in the liver, and a large region of liver parenchyma available for LSM (Fig 4) (6,7). Table 1 summarizes issues to consider when evaluating MRE examinations for quality.

For the most accurate LSM, the goal is to obtain high-quality elastograms with a large amount of liver parenchyma uncovered by the 95% confidence map available to make the LSM. However, occasionally elastograms are low quality, with only a small amount of liver available for LSM, or nondiagnostic, with no liver parenchyma available for measurement (Fig 5). When lower-quality examinations occur, it is important to determine and, if possible, correct the cause so MRE can be repeated. Table 2 lists causes of lower-quality or nondiagnostic MRE examinations and proposed solutions (Figs S1–S6) (6–11). Finally, the softer liver parenchyma in normal livers (ie, LSM approximately <2.5 kPa) can attenuate waves resulting in a small region of interest (ROI) for LSM, which can simulate a low-quality examination but does not require troubleshooting or repeating (Fig 6) (7).

MRE Measurement Technique

Before LSM is performed, the wave images and color elastograms should be evaluated visually to determine if an elastogram likely depicts normal or elevated liver stiffness (LS) (7). Normal livers typically have thin waves that are attenuated (darken) as they move toward the central portion of the liver and display blue or violet liver parenchyma on color elastograms. With elevated LS, wave images demonstrate thicker waves that are unattenuated, while color elastograms depict liver parenchyma in green through red (Fig 7).

When making the LSM, each elastogram is evaluated for ROI placement. ROI measurements can be performed manually or by using automated techniques (12). Manual ROI

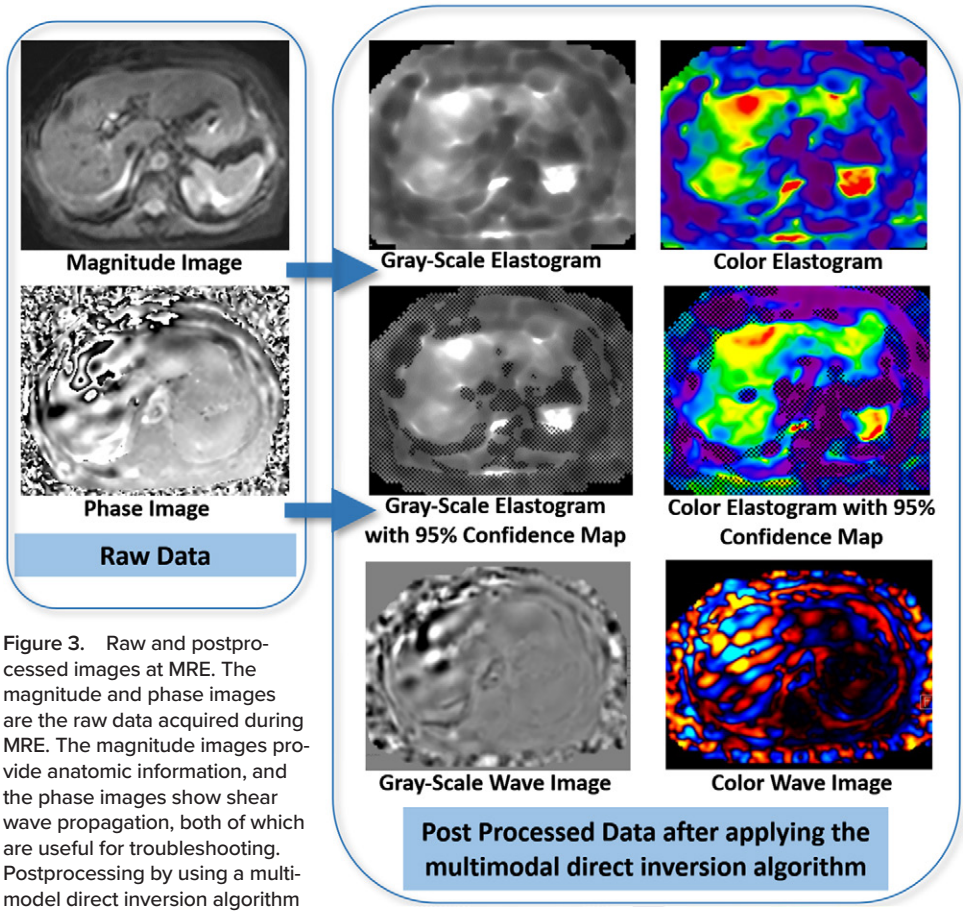

Figure 3. Raw and postprocessed images at MRE. The magnitude and phase images are the raw data acquired during MRE. The magnitude images provide anatomic information, and the phase images show shear wave propagation, both of which are useful for troubleshooting. Postprocessing by using a multimodel direct inversion algorithm generates gray-scale and color elastograms without and with a 95% confidence map and gray-scale and color wave images. Liver stiffness (LS) can be measured on either the gray-scale or color elastogram, depending on the vendor. The color images are useful for subjective and qualitative assessment of LS. (The images in Figures 3–20 are axial images.)

measurements can be performed at the MRI scanner, on a picture archiving and communication system (PACS), or on an independent workstation. ROI measurements should be made by using a freehand ROI tool, sampling the largest portion of liver on each elastogram. When making ROI measurements, the following general principles apply. On magnitude images, which are best for evaluating liver anatomy, areas within 1 cm of the liver edge, large vessels, extrahepatic tissues, fissures, masses, and gallbladder fossa should be avoided. On wave images, areas with wave distortion, low-amplitude waves, and poor wave propagation should be avoided. On elastogram images, crosshatched regions on the 95% confidence map should be excluded. Finally, liver "hot spots," which usually result from shear wave interference, reflect artifact rather than actual stiffness and should be avoided (6,7,13). Hot spots frequently occur under the passive driver from excessive vibrations and along the liver dome from oblique shear wave orientation relative to the section plane (Figs S5, S6) (7). Large vessels and masses can also cause hot spots.

The method for making the LSM varies depending on the PACS or workstation features such as the availability of an ROI copy-and-paste function and confidence map (Figs 8–10). For analysis of liver MRE examinations, ROIs are drawn on each image and the mean LSMs *(m)* in kilopascals are recorded. The areas *(a)* of the ROIs are also recorded. The measurements are combined into an overall mean LSM. This can be done by calculating a simple average of the mean stiffness values on each image. However, calculating the weighted mean (ie, weighted arithmetic mean) corrects for the different sizes of the ROIs on each image and will avoid potential measurement bias if some ROIs are much smaller than others. To calculate the weighted arithmetic mean, AM_w, the following formula can be used:

$$AM_w = (m1a1 + m2a2 + m3a3 + m4a4) \div (a1 + a2 + a3 + a4)\ (\text{Fig 11})\ (8).$$

MRE Interpretation

The overall mean LSM and a range of LSM values can be included in the radiology report. The report should include a reminder that LSM values need to be interpreted in conjunction with clinical and laboratory results because confounding factors can affect LS unrelated to fibrosis (Table 3) (11,14–17). For example, LS can increase after meal ingestion, and therefore fasting is recommended for patients 4–6 hours before elastography is performed (18–20). With heterogeneously fibrotic livers, it may be best to measure the largest liver area possible to obtain the overall LS and also report the LSM range (21). MRE results should be reported to the nearest decimal (eg, 2.3 kPa,

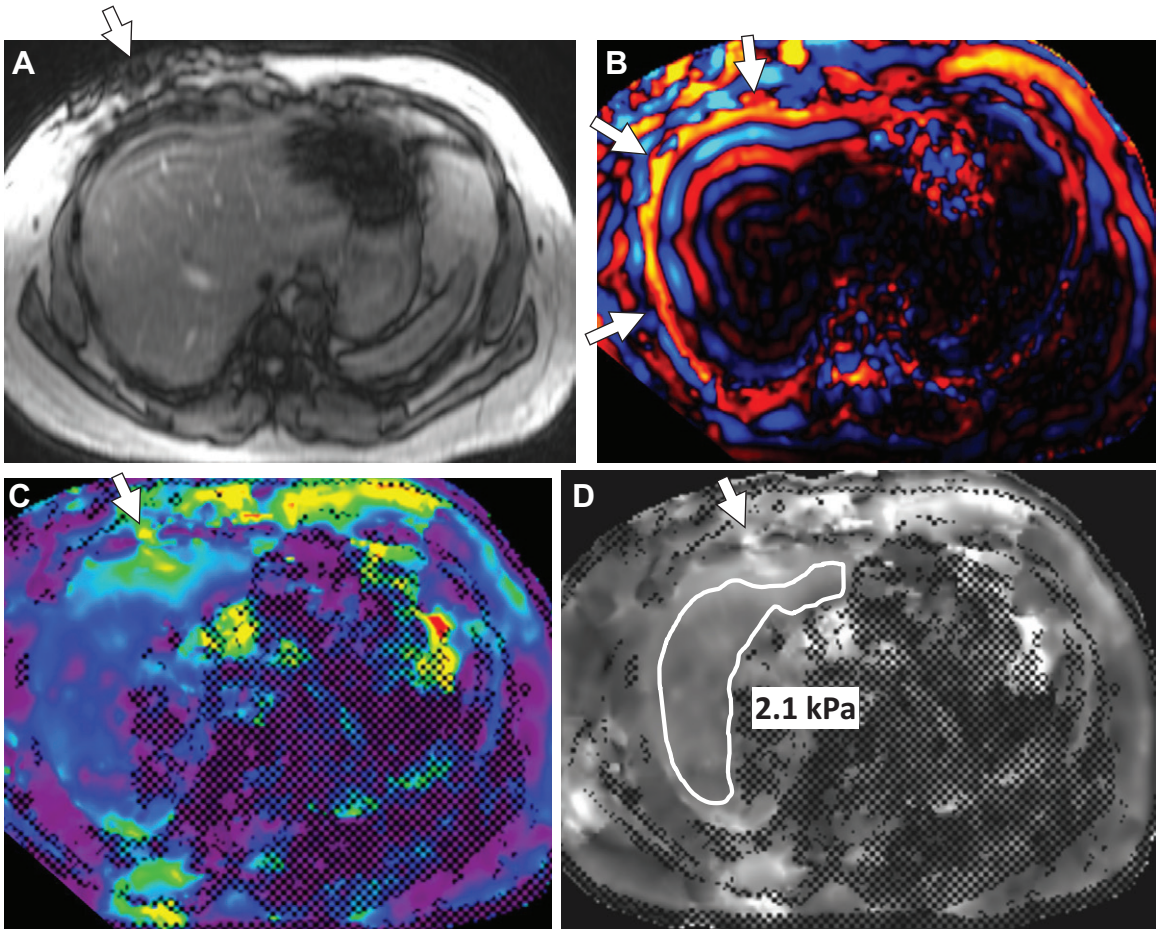

Figure 4. Features of a good-quality MRE examination. **(A)** Magnitude image obtained through the mid liver shows signal void in the abdominal wall (arrow). **(B)** Wave image shows good-quality waves that propagate through the liver (arrows) with minimal wave distortion. **(C, D)** Color **(C)** and gray-scale **(D)** elastograms show a large area of the liver uncovered by the 95% confidence map, available for LSM. On the confidence maps, the crosshatched regions indicate areas with low-confidence data that should be excluded when making the LSM. The ROI on image **D (outline)** shows an LSM of 2.1 kPa, which is within the normal range. There is a hot spot under the passive driver on the elastograms (arrow in **C** and **D**), which was excluded from the LSMs. Liver hot spots are usually due to shear wave interference and reflect artifact rather than actual LS.

Table 1: Issues to Consider When Evaluating MRE Examinations for Quality

Magnitude series
Is there signal void in the abdominal wall?*
Were sections obtained through the mid liver?*
Is the overall liver signal intensity decreased?
Is significant motion artifact or ascites present?
Is bowel interposed between the passive driver and liver?
Wave series
Is there good wave propagation?*
Is there focal or diffuse wave distortion?
Are there low-amplitude (dark) waves?
Is there artifact from the lung base or susceptibility effect of bowel gas present?
Elastograms
Is enough liver parenchyma available to make LSMs?*
Are artifactual hot spots present?

*Features of a good-quality MRE examination.

not 2.34 kPa). Figure 12 provides a dictation template that can be added to a diagnostic MRI report or used as a stand-alone report.

Quantification of Liver Fat and Iron with MRI

Overview

MRI techniques to quantify liver fat and iron concentration have been available and approved for clinical care for over 10 years. These MRI-derived biomarkers have been adopted into clinical management guidelines (22), resulting in increasing clinical demand in academic centers and community practices alike.

Currently considered the most objective MRI metric of tissue fat content, the proton density fat fraction (PDFF) is the ratio of mobile protons in fat (triglyceride) molecules to the total mobile protons of water and fat (23,24). Several methods are available to measure the liver PDFF (eg, MR spectroscopy), but the most widely used is based on a chemical shift–encoded (CSE) multiecho spoiled gradient-recalled-echo (mSGRE) sequence. Several different MRI biomarkers of liver iron quantity have been proposed (25–28). Of these, the mSGRE-based

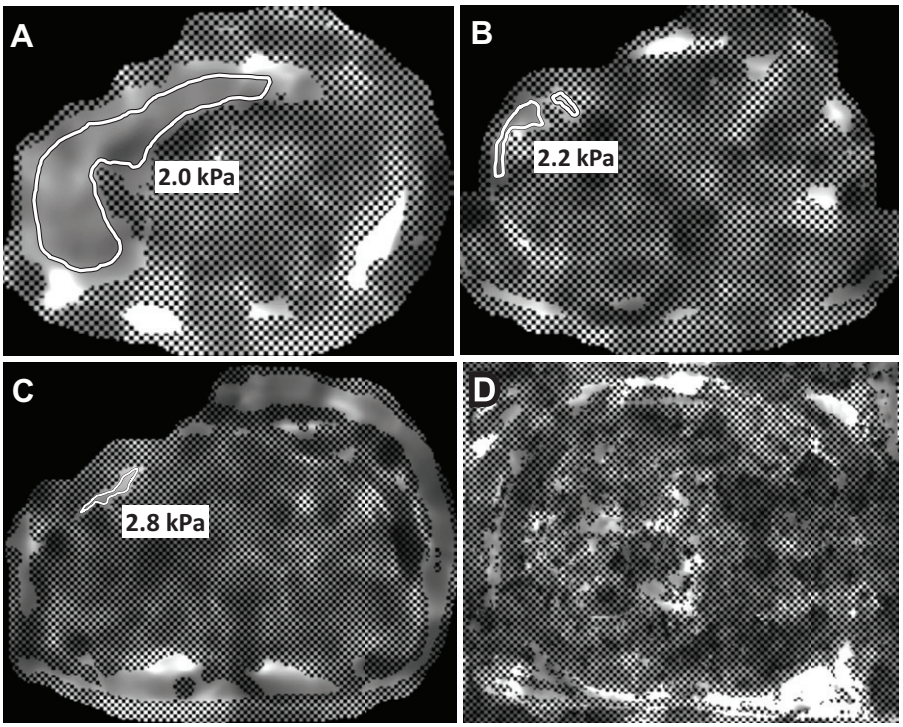

Figure 5. High-quality, low-quality, and nondiagnostic gray-scale elastograms in four patients. **(A)** High-quality elastogram shows a large amount of liver available for LSM within the ROI (outline). **(B, C)** Low-quality elastograms in two patients show a small amount of liver parenchyma available to make LSMs on both elastograms, with small ROI measurements (outline) drawn on both images. The cause of both of these low-quality images was mild liver iron overload obtained with gradient-echo sequences. **(D)** Nondiagnostic elastogram shows the crosshatching of the 95% confidence map covering the entire liver and no liver available for LSM.

transverse relaxation rate (R2*) is emerging as the first-line biomarker of liver iron concentration and is naturally bundled with PDFF measurements by using the CSE MRI method. In this section, we review the basic principles of fat and iron MRI biomarkers, the pulse sequences that allow biomarker estimation, and the interpretation of PDFF and R2* parametric maps (Appendix S1).

MRI-based Liver Fat Quantification

Hepatic steatosis is the histologic hallmark of fatty liver disease, defined as the abnormal intracellular accumulation of triglycerides within hepatocytes (29,30). Tissue triglyceride concentration can be measured by exploiting the difference in the MR frequencies, or chemical shift, between triglyceride and water protons. This is the basis of conventional T1-weighted dual-echo in- and opposed-phase (IOP) MRI, where echo times (TEs) are chosen such that the signal contributions of protons from water and those from methylene protons on fat are either in-phase (ie, additive) (TE ~2.3 msec at 3 T; 4.6 msec at 1.5 T) or opposed-phase (ie, subtracting) (TE ~1.15 msec at 3 T; 2.3 msec at 1.5 T). IOP imaging allows subjective assessment of hepatic steatosis by detecting relative signal loss on opposed-phase images. CSE fat-water separation takes this one step further to computationally synthesize T1-weighted fat-only and water-only images, from which a fat fraction (FF) map can be calculated as $FF = S_{fat} / (S_{fat} + S_{water})$, where S is the observed signal intensity of fat-only and water-only images as labeled (31,32). In tissues with low fat content, FF can also be calculated as $(S_{ip} - S_{op}) / 2 \times S_{ip}$, where S is the observed signal intensity of in-phase (ip) and opposed-phase (op) images as labeled. However, these calculations from observed signal intensities are biased by multiple confounders—notably T1 bias, T2* decay, and the spectral complexity of fat (33). Objective and standardized fat quantification requires eliminating these confounders (24). The confounder-corrected FF is referred as the PDFF, representing the ratio of mobile triglyceride protons to all mobile protons and is a chemical measure of tissue triglyceride concentration (34), calculated as $PDFF = PD_{fat} / (PD_{fat} + PD_{water})$. PDFF has been validated against liver biopsy and MR spectroscopy as reference standards and has shown excellent reproducibility across a variety of field strengths and vendors in several meta-analyses (35–37).

PDFF technique is usually implemented as an mSGRE sequence, using low flip angle radiofrequency excitation to minimize T1 bias, T2* decay correction over six sequential TEs, and multipeak triglyceride spectral modeling (Fig 13). The dedicated reconstruction algorithm can generate several types of calculated images, including in- and opposed-phase images, water PD and fat PD images, and the PDFF map (Figs 14, 15). As PDFF calculation requires the estimation of correction of T2* signal decay, a T2* (or alternatively R2*) map can also be reconstructed, the implication of which is discussed in the next section. Current commercial implementations, such as IDEAL-IQ (GE Healthcare), qDixon (Siemens Healthineers), and mDixon Quant (Philips Healthcare), use three-dimensional (3D) Cartesian k-space sampling within 10–20-second breath holds and are available at both 1.5 T and 3 T. Rapid compressed sensing k-space sampling sequences and free-breathing motion-robust sequences have been developed and are expected to become available in the near future for patients who have difficulty with breath holding (38–41).

MRI-based Fat Quantification Measurement Technique and Interpretation.—PDFF maps are interpreted by placing multiple circular ROIs (diameter ≥2 cm) onto the liver PDFF maps, while avoiding large vessels, focal lesions, artifacts, and the liver edge (42). For high interreader reproducibility, at least

Table 2: Causes of Lower-Quality or Nondiagnostic MRE Examinations and Proposed Solutions

Cause	Magnitude Images	Wave Images	Elastograms	Solution
Poor or No Shear Wave Delivery to the Liver				
Connecting tube disconnected	No signal void in abdominal wall	No shear waves	Nondiagnostic	Reconnect the tube and secure connection
Active driver powered off	No signal void in abdominal wall	No shear waves	Nondiagnostic	Power on the active driver
Passive driver loose or not in contact with the abdominal wall	Minimal or no signal void in abdominal wall	Minimal low-amplitude waves	Small ROI for LSM	Place the passive driver snugly on the abdominal wall over liver
Driver amplitude set too low	Minimal or no signal void in abdominal wall	Minimal low-amplitude waves	Small ROI for LSM	Increase amplitude to appropriate level for patient size
Interposing structures between the passive driver and liver	Colon or other structure between passive driver and liver	Wave distortion and low-amplitude waves	Small ROI for LSM	Reposition the driver so that it lies over the liver and repeat MRE
Shear Waves Delivered but Lower-Quality Elastogram Obtained: Patient Conditions				
Iron overload	Decreased liver signal intensity	No shear waves within the liver	Nondiagnostic	Use lower echo time (TE) Use spin-echo echo-planar imaging pulse sequence (if available) Use 1.5-T scanner (if available)
Moderate to severe hepatic steatosis	Slightly decreased liver signal intensity	Lower-amplitude waves with wave propagation	Moderate-sized ROI for LSM	Use in-phase TE or reduce TE closer to in-phase
Massive ascites	Massive ascites	Chaotic waves	Nondiagnostic	Use 1.5-T scanner (if available) to decrease dielectric effect Consider large-volume paracentesis before imaging
Shear Waves Delivered but Lower-Quality Elastogram Obtained: Technical Reasons				
Elastogram sections obtained too high or too low	Elastogram sections obtained too high or too low	Distorted low-amplitude waves	Small ROI for LSM	Reposition passive driver to obtain sections through mid liver
Driver amplitude set too high	Signal void on abdominal wall extends into the liver	Wave distortion (phase wrap)	Hot spot under passive driver to be excluded from LSMs	Decrease the amplitude to the appropriate level for patient size
Patient motion artifact	Blurry image with motion artifact	Wave distortion	Small ROI for LSM	Encourage patient breath holding Use spin-echo echo-planar imaging pulse sequence (if available)

four ROIs should be placed whenever possible, two or three in the right lobe and one or two in the left lobe, in representative areas of liver parenchyma (Fig 16). The placement of ROIs in the left lobe may be challenging owing to smaller size and cardiac motion artifact.

The mean PDFF value is reported (42). With PDFF, weighted or unweighted mean calculations are acceptable. A range of PDFF values could be reported when heterogeneous steatosis is present. With PDFF thresholds, there is no clear consensus in the literature for differentiating normal from abnormal values. Even reported clinical biopsy grades have no defined relationship between biopsy steatosis grade and any disease state. In the fat quantification dictation template included in Figure 12, the PDFF thresholds provided are commonly used in clinical practice and are based on the biopsy versus CSE-MRI study by Tang et al (Table 4) (43). However, more research is needed, and PDFF thresholds used when reporting cases may change in the future. PDFF results should be reported to the nearest integer (eg, 10%, not 10.4%).

MRI-based Fat Quantification Pitfalls.—In some MRI systems, scanner software versions, or image viewers, the ROI value may need to be scaled by a factor of 10. This can be checked by placing an ROI in the subcutaneous fat, which should have PDFF values of 80%–100%, typically 93%–96% (Fig 16). PDFF values are independent of field strength, and ROI values do not need to be modified in this respect, unlike liver iron concentration calculation, as discussed in the next section.

The CSE fat-water separation technique that underpins PDFF is susceptible to a unique artifact referred to as fat-water swap. The artifact is a result of the natural ambiguity of the signal from water or fat dominant voxels during the computational

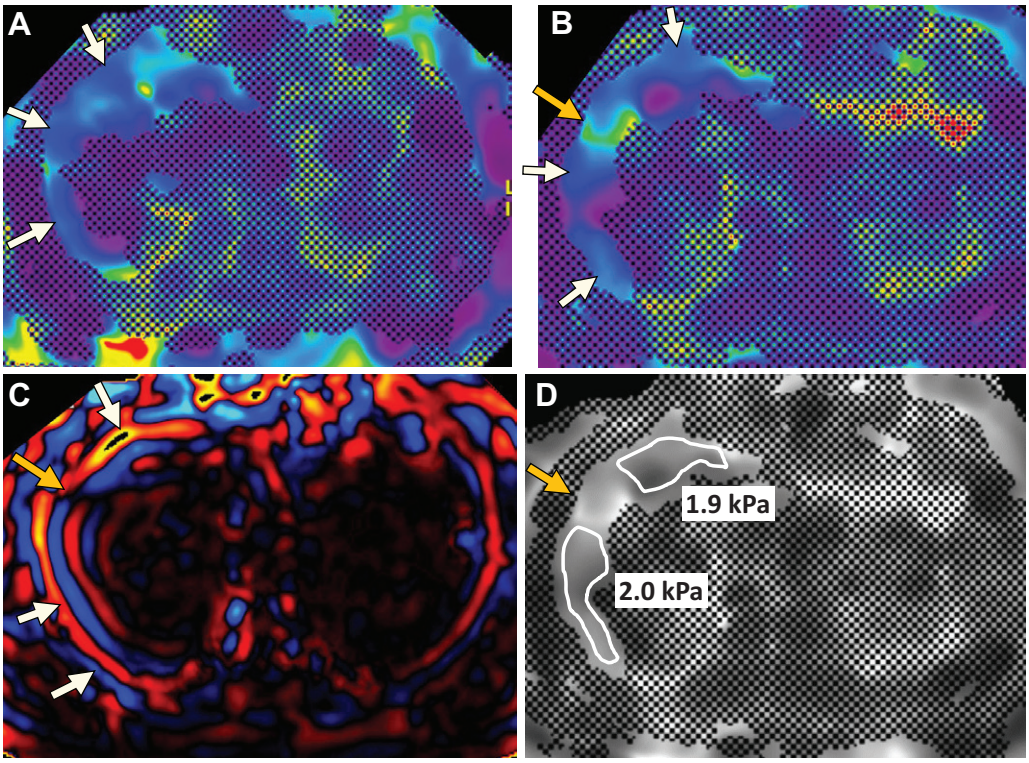

Figure 6. Normal MRE simulating a lower-quality examination. **(A, B)** Color elastograms from two different section locations in the same patient show that the liver parenchyma appears mostly blue throughout, indicating lower stiffness values (white arrows). **(C)** Wave image corresponding to **B** shows waves that are relatively thin (white arrows) and darken centrally owing to attenuation from softer normal liver parenchyma. **(D)** Gray-scale elastogram corresponding to **B** (excluding a hot spot) shows ROI measurements (outline) with normal LS values. While the smaller size of the ROI for this normal MR elastogram simulates a lower-quality image, this examination does not require troubleshooting or repeating. Note that the gold arrow on **B** and **D** indicates an elastogram hot spot caused by wave distortion (gold arrow on **C**). This hot spot region was not included in LSMs.

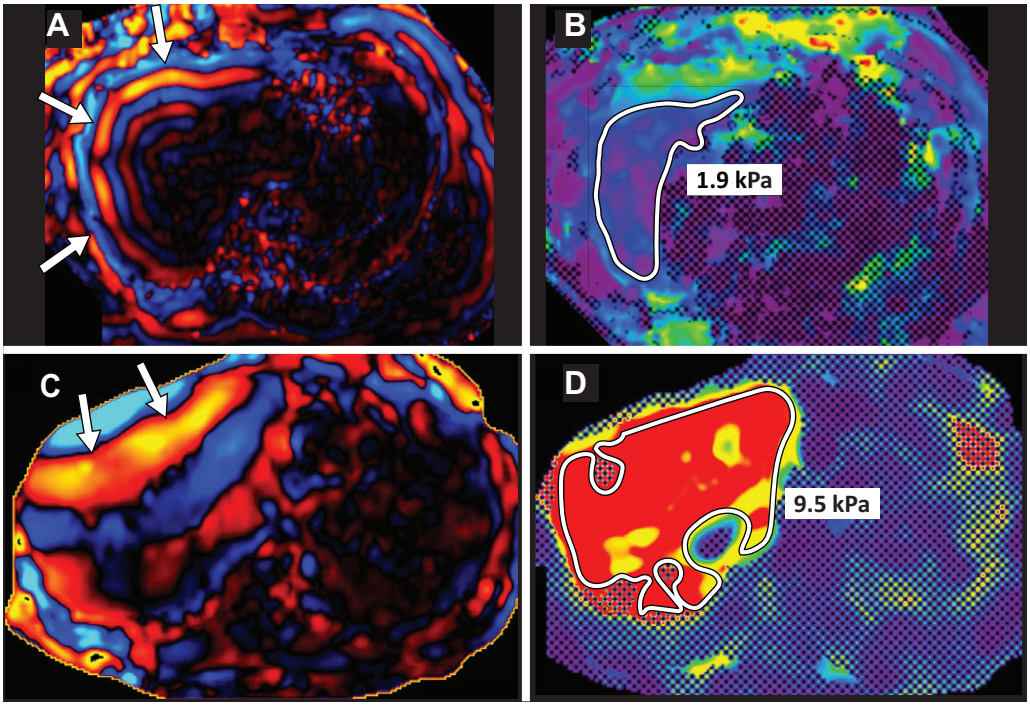

Figure 7. Healthy nonfibrotic **(A, B)** versus fibrotic **(C, D)** liver. **(A)** Wave image in a healthy nonfibrotic liver shows thin waves (arrows) that darken centrally as they are attenuated by softer normal liver parenchyma. **(B)** Color elastogram shows that the liver tissue not excluded by the 95% confidence map is blue or violet owing to lower stiffness values. The LSM was 1.9 kPa for this section, which is within the normal range. **(C)** Wave image in a fibrotic liver in a different patient shows waves (arrows) that are thicker than those on **A** and not attenuated centrally. **(D)** Color elastogram shows that the liver tissue not covered by the 95% confidence map is red or orange owing to elevated stiffness values. The LSM for this section is 9.5 kPa, which is consistent with stage 4 fibrosis or cirrhosis.

step to separate the relative signal contributions by fat and water, which can result in incorrect assignment of water signal as fat and fat signal as water. Fat-water swaps can affect only a portion of a single image or the entire series (Figs 17, 18). ROIs should not be placed in swapped areas as the PDFF values are incorrect. However, if only a portion of the liver is affected, the remainder of the unswapped liver can be used for ROI placement. Another type of artifact occurs in severe liver iron overload, where PDFF estimation becomes impossible due to insufficient signal-to-noise ratio (SNR) in the later TE images of multiecho CSE acquisitions. This is further explained in the next section.

MRI-based Liver Iron Quantification

Due to the ferromagnetic property of iron, the MR signal in iron-loaded liver decays more rapidly than does the normal liver. This decay rate can be quantified by the transverse relaxation times (T2 and T2*, both reported in milliseconds) or rates (R2 and R2*, both reported in inverse seconds). The

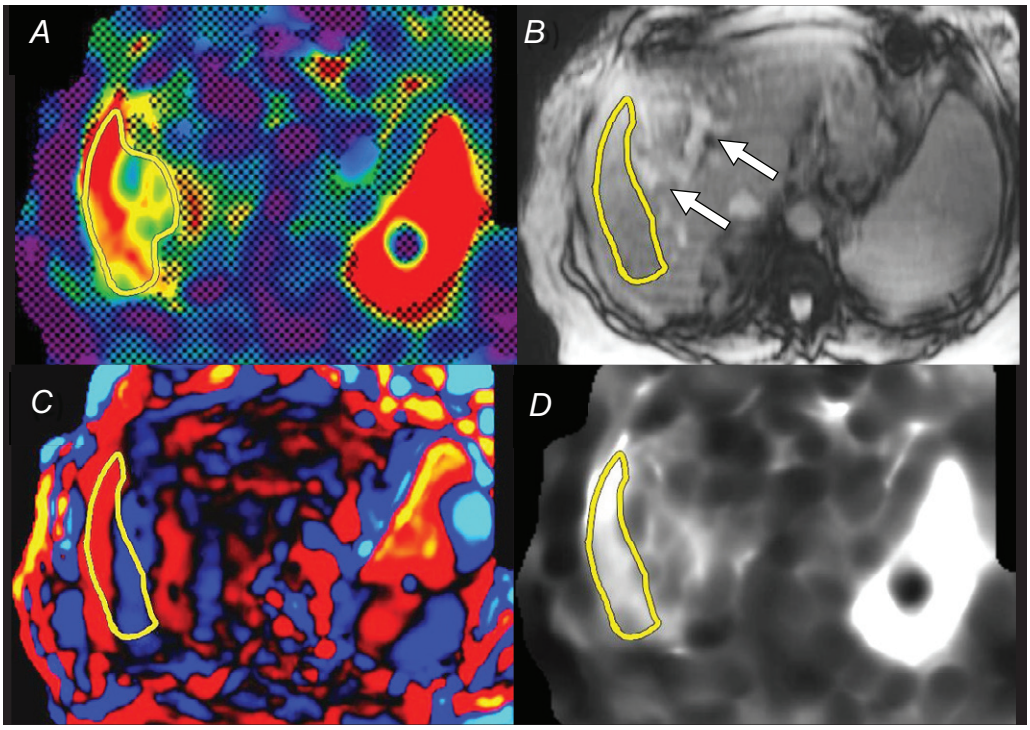

Figure 8. How to make LSMs when both a copy-and-paste function and confidence map are available. First, an ROI (outline in *A–D*) is drawn on the color elastogram, *A*, with confidence map, avoiding the cross-hatched regions. This ROI is then copied and pasted onto the magnitude image, *B*, with adjustments made to avoid large vessels (arrows) and the liver edge. Next, the ROI is copied onto the color wave image, *C,* to ensure good-quality waves are being sampled, with adjustments made to avoid areas of wave distortion. Finally, the ROI is copied to the gray-scale elastogram*, D,* to obtain the LSM for this section. This process is repeated for all sections obtained, and then the weighted arithmetic mean is calculated to determine the overall mean LSM. The overall mean LSM was 7.0 kPa, which is within the stage 4 fibrosis or cirrhosis range.

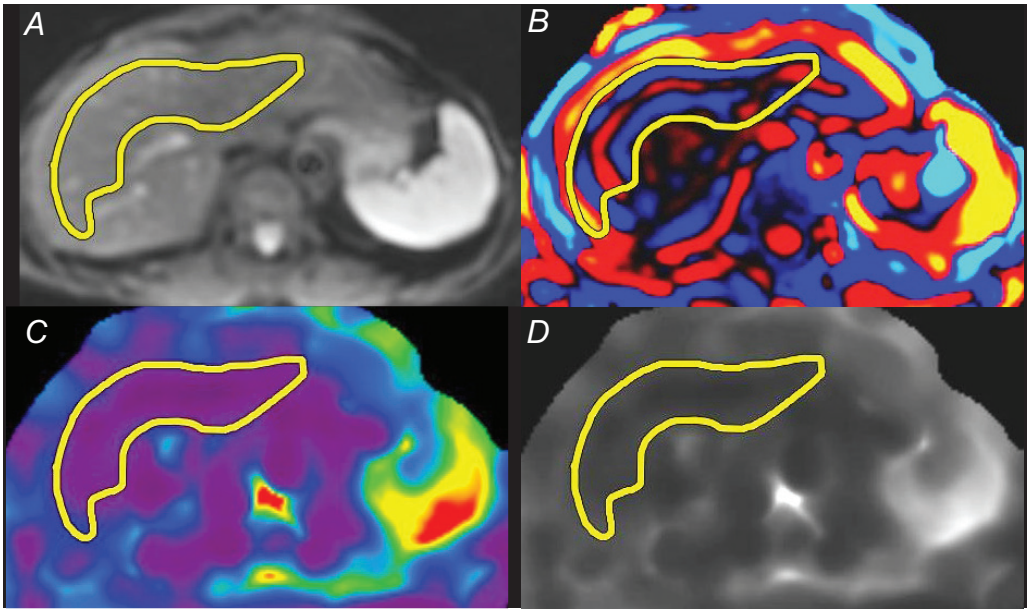

Figure 9. How to make LSMs when a copy-and-paste function is available but a confidence map is not. First, an ROI (outline in *A–D*) is drawn on the magnitude image*, A,* avoiding the liver edge and large vessels. This ROI is then copied and pasted onto the color wave image, *B*, to ensure good-quality waves are being sampled, with adjustments made to avoid areas of wave distortion. Finally, depending on the MRI system used, the ROI can be copied onto the color elastogram, *C*, or gray-scale elastogram, *D,* to obtain the LSM for this section. This process is repeated for all sections obtained, and then the weighted arithmetic mean is calculated to determine the overall mean LSM. The overall mean LSM in this patient was 1.5 kPa, which is within the normal range.

measurement of these relaxation times or rates is referred to as *relaxometry*. R2 mapping is performed by pixel-by-pixel biexponential model relaxometry on the signal intensity data from multiple spin-echo (SE) acquisitions at different TEs, resulting in an R2 map of the liver. Average liver R2 values have been calibrated against liver iron concentration (LIC, in milligrams of iron per gram [mg Fe/g] or micromole of iron per gram [μmol Fe/g] of dry liver tissue) measured by a biochemical assay from liver biopsy specimens and shown to be reproducible (44–46). An increase in LIC results in a *nonlinear*, although monotonic, increase in liver R2. Published nomograms can be used to estimate LIC from the measured average R2 value. Long acquisition times, limited number of sections, motion artifact, and added time and cost of off-line proprietary analysis are limitations of current commercially available R2 relaxometry techniques (eg, FerriScan; Resonance Health).

R2* relaxometry is performed by pixel-by-pixel single-exponential model relaxometry on the signal-intensity data from an mSGRE acquisition, resulting in a liver R2* map (47). The most convenient method of obtaining a liver R2* map is by using commercially available CSE mSGRE sequences, which simultaneously generate volumetric PDFF and R2* maps in a single breath hold (48). The simultaneous quantification is important, as accurate R2* estimation requires elimination of the confounding effects of fat (and vice versa) (49). Unlike SE-based R2 relaxometry, an increase

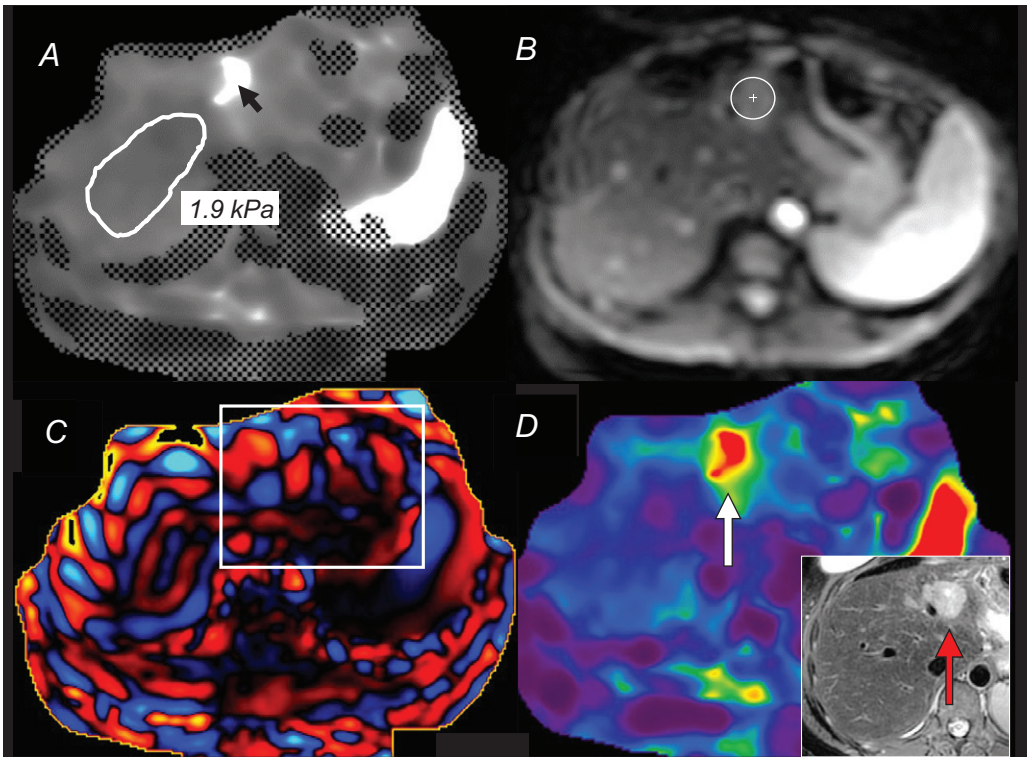

Figure 10. How to make LSMs when a confidence map is available but a copy-and-paste function is not. The first step, using a "localizer mode," is to hover the cursor (arrow in *A*) on the gray-scale elastogram with confidence map to identify corresponding areas marked by a crosshair on the magnitude image (circle in *B*). Use this function to avoid the liver edge, fissures, large vessels, and masses when drawing the ROI (outline in *A*). Next, on each wave image, identify areas with wave distortion (rectangle in *C*), low-amplitude waves, and poor wave propagation, and avoid inclusion in the ROI. Finally, hot spots identified on the color elastogram (white arrow in *D*) are avoided. The hot spot in *D* was caused by a liver metastasis, confirmed by correlating the finding with that on a fat-suppressed T2-weighted MR image (red arrow in inset image). Free-hand ROI measurements are then made on the gray-scale elastogram with confidence map, *A*, for each of the four sections to obtain the LSM for each section, and then the weighted arithmetic mean is calculated to determine the overall mean LSM. The overall mean LSM was 1.9 kPa, which is within the normal range.

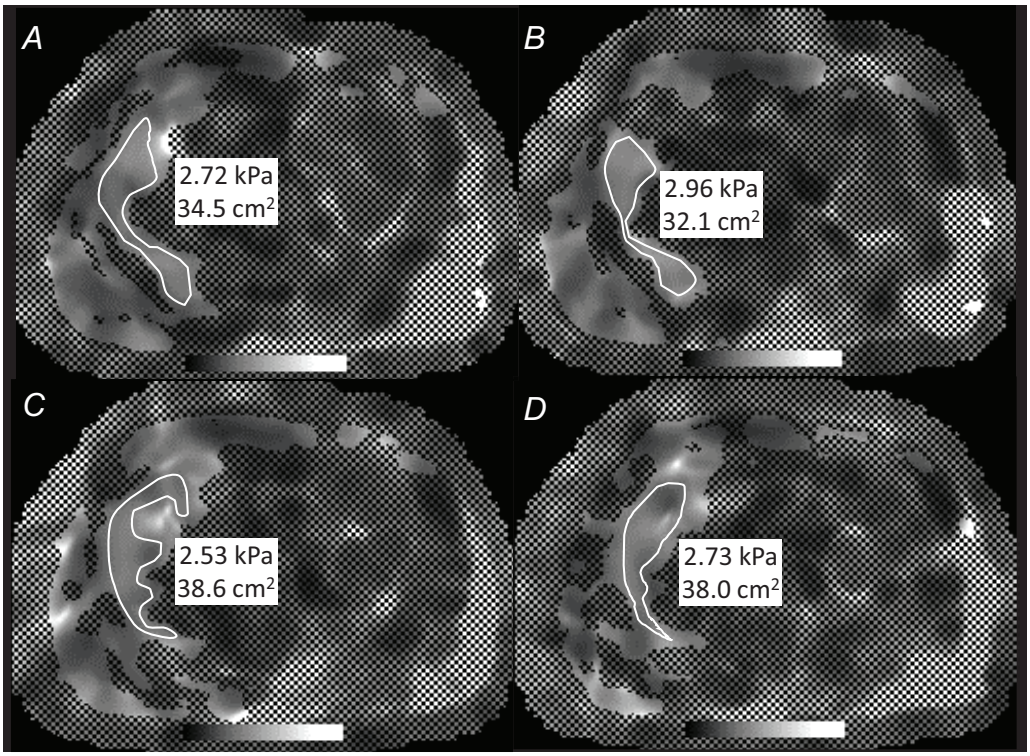

Figure 11. How to calculate the weighted arithmetic mean for LSMs. The weighted arithmetic mean reflects the relative contribution of the area of the liver measured in each section. LSM can be reported as the weighted arithmetic mean along with the range of values. For the analysis of liver MRE examinations, ROIs are drawn on each section and the mean LSMs (*m*) in kilopascals are recorded, as depicted on the gray-scale elastograms, *A*–*D*. The areas (*a*) of the ROIs are also recorded. To calculate the weighted arithmetic mean (AM_w), the following formula can be used: $AM_w = (m1a1 + m2a2 + m3a3 + m4a4) \div (a1 + a2 + a3 + a4)$. For this patient, calculation of the weighted arithmetic mean LSM is as follows: $[(2.72 \times 34.5) + (2.96 \times 32.1) + (2.53 \times 38.6) + (2.73 \times 38.0)] \div (34.5 + 32.1 + 38.6 + 38.0) = 2.73$ kPa. Thus, for this examination, the overall mean LS to report is 2.7 kPa (range, 2.5–3.0 kPa).

in LIC results in a *linear* increase in R2* (47,50). R2* relaxometry for LIC estimation has recently undergone a multicenter multivendor validation and was found to be repeatable and reproducible at 1.5 T, 2.89 T, and 3.0 T (51). Unlike commercial R2 relaxometry, which requires off-site analysis, mSGRE R2* maps can be automatically reconstructed and sent to a radiology workstation for immediate interpretation. As such, many radiology practices have adopted R2* relaxometry as the first-line method for MRI-based liver iron quantification.

MRI-based Iron Quantification Measurement Technique and Interpretation.—The reconstructed R2* map is usually interpreted and analyzed by placing ROIs. At this time, evidence-based consensus of ROI placement has not been published, but

Table 3: Confounders That Affect LSM with Both MRE and US SWE*

Factor	Effect on LSM	How to Identify	Effect on Interpretation
Acute hepatitis, elevated transaminases, flares of hepatitis in patients with hepatitis B or C infection	Elevated LSM	AST and/or ALT can be up to five times greater than normal value	Overestimates the degree of fibrosis
Elevated right heart pressure (congestive heart failure, tricuspid regurgitation) or Fontan palliation	Elevated LSM	Enlarged IVC and hepatic veins, medical records, cardiac status	Overestimates the degree of fibrosis; it is not possible to use cutoff values, as the degree of congestion and its contribution to stiffness is unknown
Nonfasting state	May lead to elevated LSM	Contracted gallbladder	Overestimates the degree of fibrosis; if the LSM is within normal range, no need to repeat the examination in the fasting state
Budd-Chiari syndrome	Elevated LSM	Evaluate hepatic veins	Overestimates the degree of fibrosis
Infiltrative diseases (amyloidosis, sarcoidosis, diffuse liver metastasis, Gaucher disease)	Elevated LSM	Medical records, patient history	Overestimates the degree of fibrosis
Alcohol abuse, alcohol binge	Elevated LSM	Medical records, patient history	Overestimates the degree of fibrosis
Acute biliary obstruction	Elevated LSM	Findings at B-mode US, CT, or MRI	Overestimates the degree of fibrosis
Treatment of hepatitis C with DAAs†	Decreased LSM	Medical records	With treatment, the degree of inflammation decreases, decreasing LSM over a few weeks; fibrosis might start to improve over several months
Hepatitis B infection undergoing treatment	Decreased LSM	Medical records	Pattern of LSM decline likely reflects remission of liver inflammation and fibrosis regression during the first 6 months and fibrosis regression during long-term antiviral therapy

Note.—ALT = alanine aminotransferase, AST = aspartate aminotransferase, DAAs = direct antiviral agents, IVC = inferior vena cava.
* For any of the confounders, the delta change in LS may be helpful in assessing the progression or regression of disease, regardless of the cause.
† In patients with chronic hepatitis C infection treated with DAAs, the baseline value must be the one obtained at the end of treatment.

many centers have adopted similar methodology as for PDFF (Fig 19). Once ROIs are placed, the mean R2* value for the ROIs is calculated and reported. Similar to PDFF, weighted or unweighted mean calculations are acceptable. A range of R2* values may be reported if there is heterogeneous distribution across the liver. R2* values are then converted to LIC in milligrams of iron per gram of (mg Fe/g) dry liver tissue by using field-specific calibration equations (Table 5) (51). Care must be taken to use the correct equation for each field strength. If the LIC is reported in micromole of iron per gram of (μmol Fe/g) dry liver tissue, the LIC value in mg Fe/g can be converted to μmol Fe/g by dividing by 0.055845, which is the atomic weight of iron (ie, 0.055845 mg/μmol or 55.845 g/mol).

LIC can be used to grade liver iron overload severity (Table 6) (46). It is important that R2* LIC measurement is reported in a standardized format to aid patients and referring clinicians. If prior LIC values are available, providing comparison with the current LIC value is recommended to help clinicians assess the evolution of disease (52–56). R2* and LIC results should be reported to the nearest integer (eg, 76/sec, not 76.2/sec) and decimal (eg, 18.2 mg Fe/g, not 18.23 mg Fe/g), respectively. A dictation template for reporting results is provided in Figure 12.

MRI-based Iron Quantification Pitfalls.—The standard CSE mSGRE sequence used for PDFF is usually suitable for accurate R2* LIC estimation in patients with mild or moderate iron overload. However, in patients with severe or extreme iron overload, the signal may decay too fast for the mSGRE acquisition to measure the liver signal intensity adequately before it decays to noise. When this occurs, the R2* estimation becomes computationally unstable, resulting in imprecise estimates and a speckled "snowstorm" appearance on the R2* map (Fig 20). It is important to recognize this appearance and not use the R2* maps for LIC measurement. In addition, the accompanying PDFF map is uninterpretable because the accuracy of PDFF estimates and R2* estimates are interdependent. This situation can often be remedied by shortening the initial TEs to less than 1 msec and the interecho interval to less than 1 msec, usually achievable by reducing the acquisition matrix (thus spatial resolution) or by using fractional echoes and/or an interleaved acquisition (ie, even and odd TEs acquired in two separate repetition times). Otherwise, alternative LIC estimation methods can be considered, such as an R2-based LIC method (FerriScan) or liver biopsy.

US SWE

Overview

US SWE techniques include vibration-controlled transient elastography (VCTE) and acoustic radiation force impulse

PROCEDURE: [GRE/SE EPI] MR elastography and chemical shift-encoded GRE sequences were performed for liver fibrosis, fat, and iron quantification on a [1.5/3.0/2.89] Tesla scanner.

MR Liver Elastography

Mean liver stiffness (weighted mean of [ ] measurements): [ ] kPa (range [ ] – [ ] kPa).

Interpretation of MR elastography results. Mean LSM:

- <2.5 kPa = Normal
- 2.5 to 3.0 kPa = Normal or inflammation

Increased liver stiffness, in the appropriate clinical setting, is compatible with liver fibrosis as below:

- 3.0 to 3.5 kPa = Stage 1–2 fibrosis
- 3.5 to 4.0 kPa = Stage 2–3 fibrosis
- 4.0 to 5.0 kPa = Stage 3–4 fibrosis
- >5.0 kPa = Stage 4 fibrosis or cirrhosis

MR Liver Fat Quantification

In representative areas of the liver, the mean proton density fat-fraction (PDFF) is [ ]% (range [ ] – [ ]%).

Histological steatosis grades by PDFF:

- <6% = Normal
- 6 – 17% = Mild
- 17 – 22% = Moderate
- >22% = Severe

MR Liver Iron Quantification

In representative areas of the liver, the mean transverse relaxation rate R2* is [ ]/s (range [ ] – [ ]/s) at [1.5T/3.0T/2.89T], corresponding to a liver iron concentration (LIC) of [ ] mg Fe/g (range [ ] – [ ] mg Fe/g).

@1.5T: LIC = 0.02603 × R2* – 0.16 **@3.0T:** LIC = 0.01349 × R2* – 0.03 **@2.89T:** LIC = 0.01400 × R2* – 0.03

Iron overload severity grades by LIC:

- <1.8 mg/g = Normal
- 1.8 – 3.2 mg/g = Mild
- 3.2 – 7.0 mg/g = Moderate
- 7.0 – 15.0 mg/g = Severe
- ≥15.0 mg/g = Extreme

IMPRESSION:

1. Liver stiffness of [ ] kPa consistent with [ ].
2. [No/Mild/Moderate/Severe] hepatic steatosis with a fat fraction of [ ]%.
3. [No/Mild/Moderate/Severe/Extreme] hepatic iron overload with an estimated liver iron concentration of [ ] mg Fe/g.

Figure 12. Suggested MR liver elastography and MRI-based liver fat and iron quantification dictation template macro (6, 9, 43, 46, 51). This dictation template macro may be modified to comply with individual institutional requirements.

(ARFI) techniques (57–59). The shear waves are generated by body-surface vibrations made by a probe tip, as in VCTE, or the push-pulse of a focused ultrasound beam, as in ARFI techniques. VCTE is performed without imaging guidance when making measurements. The content of this section focuses on the imaging-guided ARFI-based techniques. This includes point SWE (pSWE), which measures stiffness in a small fixed volume of approximately 1 cc, and two-dimensional (2D) SWE, which measures stiffness over a larger user-adjustable area and includes a color-coded elasticity map that is displayed on the US monitor and sent to the PACS (Appendix S1).

For all US SWE techniques, to achieve the highest reproducibility and measurement accuracy, adherence to a strict protocol for acquiring LSM is required. However, even in the best conditions, US systems from different vendors can give different results. Therefore, the intersystem variability should be considered when comparing results (60,61). Moreover, using the same system is recommended for follow-up purposes. All guidelines recommend the same protocol for correct LSM acquisition with ARFI-based techniques (Table S1) (58,59,62,63).

US Elastography Quality Control

Optimization of the B-mode image is required, as B-mode tracks the shear waves to provide an estimate of shear wave speed (Figs 21, 22). The B-mode image should be free of artifacts, especially shadowing. The most important quality criterion is the variability between subsequent measurements, which is assessed by the interquartile range (IQR)–to-median ratio (subsequently referred to as IQR/M). The IQR/M should be less than or equal to 30% for measurements reported in kilopascals and less than or equal to 15% for measurements reported in meters per second because the conversion of meters per second to kilopascals is nonlinear (59). A high IQR/M confirms poor precision in most settings and therefore poor accuracy. However, an IQR/M in the recommended range confirms high precision but not high accuracy, as measurements taken in regions with artifacts may give a low IQR/M but are inaccurate. Using the manufacturer's quality criteria is also important to confirm that accurate LSMs have been obtained (Figs 23–25). With pSWE, 10 measurements should be obtained. Fewer than 10 measurements (at least five) can be obtained with pSWE if necessary. However, the IQR/M should be within the recommended range. For 2D SWE, five measurements should be obtained when the manufacturer's quality criteria are available.

For ARFI techniques, there can be a measurement depth dependence, so follow-up studies should be taken at the same depth. In most systems, the maximum ARFI push pulse is 4–4.5 cm from the transducer, which is the optimal location

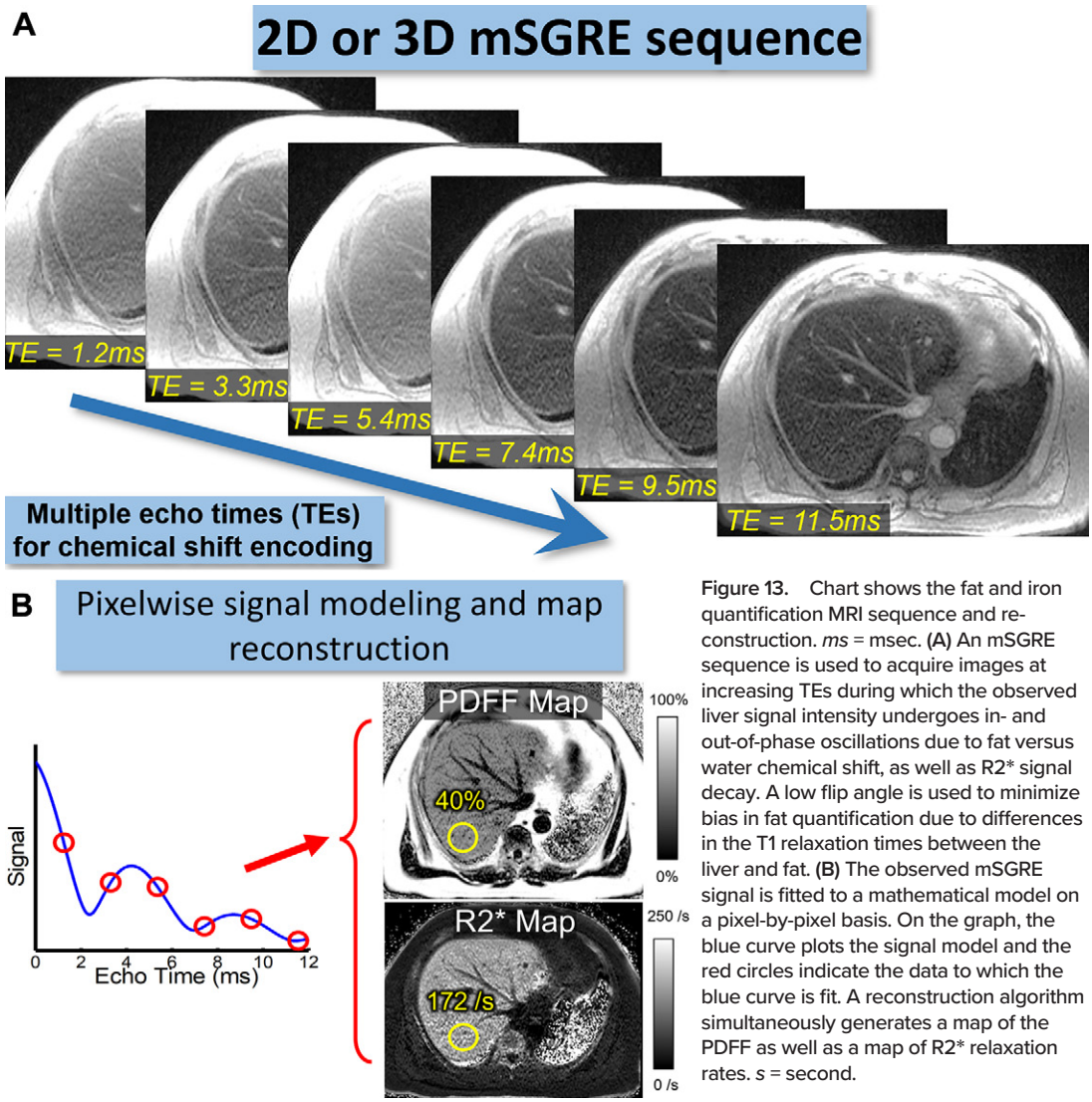

Figure 13. Chart shows the fat and iron quantification MRI sequence and reconstruction. *ms* = msec. **(A)** An mSGRE sequence is used to acquire images at increasing TEs during which the observed liver signal intensity undergoes in- and out-of-phase oscillations due to fat versus water chemical shift, as well as R2* signal decay. A low flip angle is used to minimize bias in fat quantification due to differences in the T1 relaxation times between the liver and fat. **(B)** The observed mSGRE signal is fitted to a mathematical model on a pixel-by-pixel basis. On the graph, the blue curve plots the signal model and the red circles indicate the data to which the blue curve is fit. A reconstruction algorithm simultaneously generates a map of the PDFF as well as a map of R2* relaxation rates. *s* = second.

for obtaining measurements (58,59). Recognizing artifacts is critical in performing US SWE and is discussed in the following sections.

US Elastography Interpretation

Guidelines have recommended that SWE techniques can replace liver biopsy for fibrosis staging in several clinical scenarios. However, histologic assessment and SWE do not measure the same entity. Histologic assessment evaluates fibrosis, fat, and inflammation separately, whereas SWE techniques measure LS, which is mainly related to fibrosis but also affected by inflammation, congestion, and other factors. Table 3 lists confounding factors to consider when interpreting SWE results. For many reasons, it is inappropriate to translate stiffness values into a histologic score (64). Stiffness is a quantitative estimate, whereas liver fibrosis histologic scoring systems are based on categorical scales. Therefore, even in "ideal" conditions, overlap between consecutive stages of liver fibrosis is inevitable when using LS as a liver fibrosis surrogate marker.

Several guidelines have been released for interpreting SWE measurements. A Society of Radiologists in Ultrasound (SRU) panel highlighted that the overlap between consecutive stages of liver fibrosis is as large if not larger than differences between vendors, and therefore suggested that separate cutoffs for different vendors are not required (59). In addition, the spectrum of advanced fibrosis and early cirrhosis is a continuum in asymptomatic patients, and distinguishing between the two on clinical grounds is often impossible. Considering these uncertainties, the term *compensated advanced chronic liver disease* (cACLD), which includes F3 and F4 stages, has been proposed for asymptomatic patients (65,66). Clinically, it is of utmost importance to diagnose cACLD because these patients are at higher risk of complications related to portal hypertension or hepatocellular carcinoma. Therefore, in patients with chronic viral hepatitis and nonalcoholic fatty liver disease (NAFLD), the SRU panel proposed the "rule of four" for ARFI techniques (59,63). Table 7 lists recommended interpretation guidelines for ARFI techniques. An ARFI technique dictation template is provided in Figure 26. US SWE results should be reported to the nearest decimal for LSM in kilopascals (eg, 5.3 kPa, not 5.32 kPa) and to the second decimal for LSM in meters per second (eg, 1.41 m/sec, not 1.413 m/sec). There is approximately 10% variability of US SWE measurements, and therefore at least a 10% delta change is needed for clinically relevant change (59).

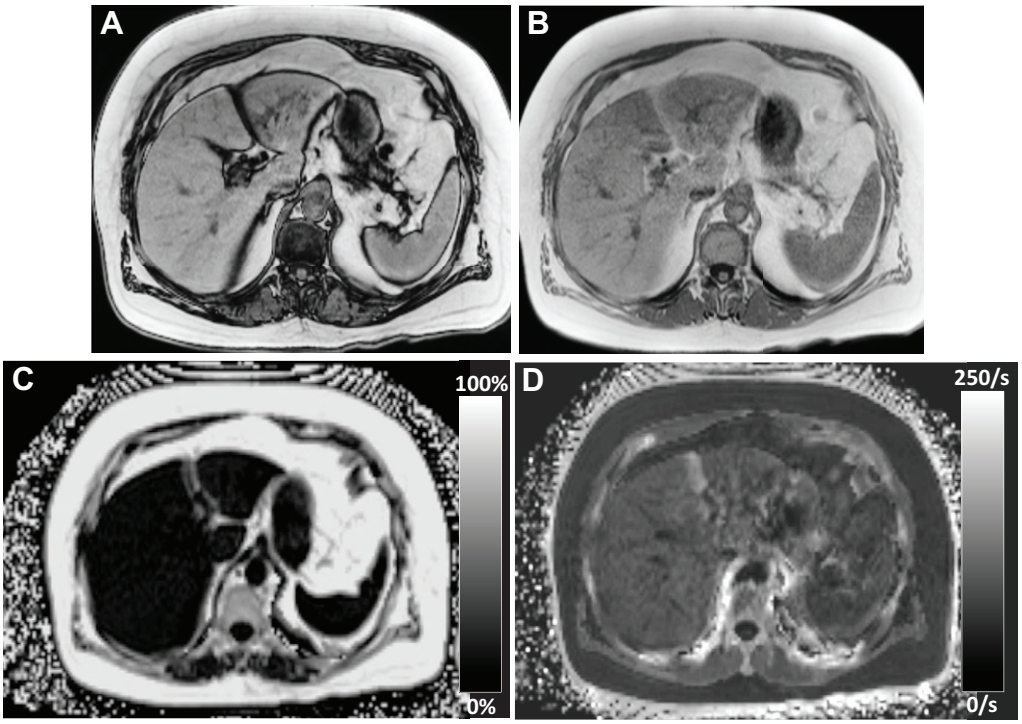

Figure 14. Typical fat-iron quantification MRI sequence output in a patient without liver fat or iron overload. These chemical shift–encoded sequences can reconstruct several types of images, including an opposed-phase image **(A)**, in-phase image **(B)**, PDFF map **(C)**, and R2* relaxation rate map **(D)**. These sequences can also generate water-only (ie, fat-suppressed) as well as fat-only (ie, water-suppressed) images (not shown). This case does not show visible signal loss on the opposed-phase image **(A)** compared with the in-phase image **(B)**, suggesting the absence of hepatic steatosis.

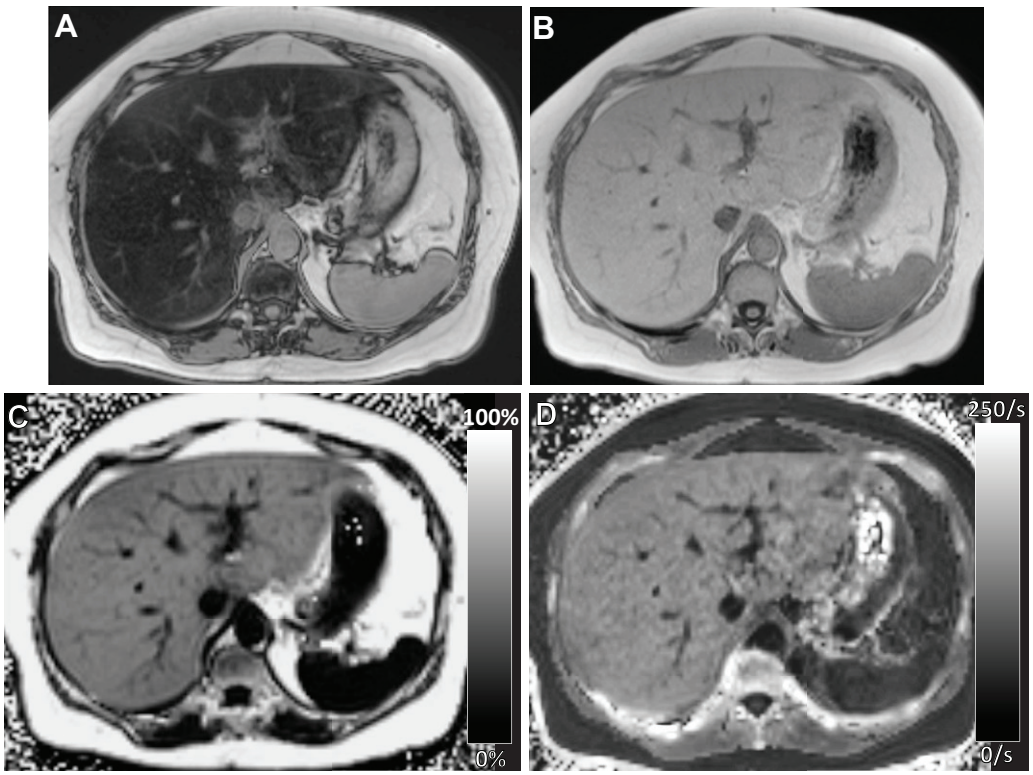

Figure 15. Fat-iron quantification MRI sequence output in a patient with liver fat and iron overload. There is marked signal loss on the opposed-phase image **(A)** compared with the in-phase image **(B)**, indicating the presence of hepatic steatosis. These qualitative observations are quantitatively confirmed by the calculated PDFF map **(C)**, where the pixel intensity (brightness) represents the PDFF, which can range from 0% (no fat, all water) to 100% (all fat, no water). There is also mildly elevated R2*, as evidenced by the brighter pixel intensities on the accompanying R2* map **(D)**. Note that elevated R2* is indicative of iron overload, which could not have been concluded based on the in- and opposed-phase images owing to obscuration of the small iron effect by a large fat effect.

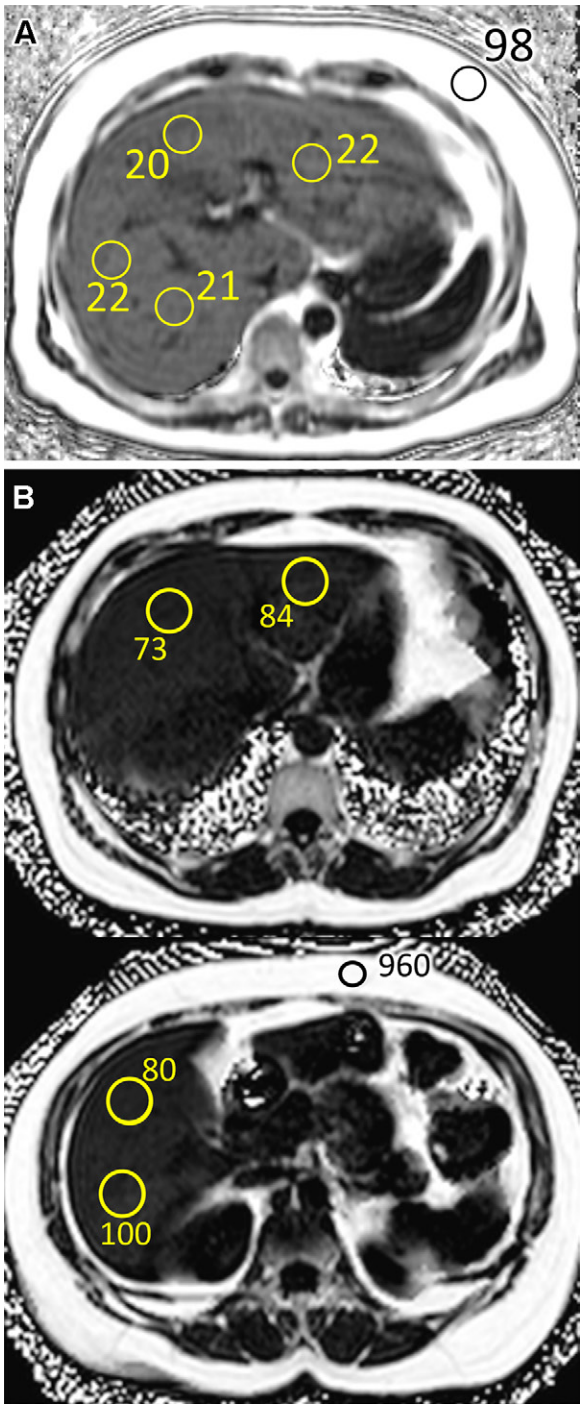

Figure 16. Examples of ROI placement on PDFF maps. At least four circular ROIs of 2 cm or larger in diameter should be drawn, two to three in the right lobe and one to two in the left lobe. Attention should be paid to avoid areas of artifact, focal lesions, visible blood vessels, and bile ducts. The average value of the four or more ROIs is reported. The ROI values can be used directly without any scaling, or scaling by a factor of 10 may be needed depending on the vendor and MRI scanner software version. For example, **A** shows a PDFF map where the ROI values can be used directly. The average PDFF value is 21%, consistent with moderate hepatic steatosis. Note that the subcutaneous fat is typically close to 100 in PDFF. **B** shows a PDFF map that is scaled by a factor of 10. The average PDFF value is 8.4%, consistent with mild hepatic steatosis. Note that the subcutaneous fat ROI value is 960, but it actually represents 96% fat after accounting for the scaling.

Table 4: PDFF Thresholds for Histologic Grades of Hepatic Steatosis

PDFF	Histologic Steatosis Grade
<6%	Normal
6%–17%	Grade 1 (mild)
17%–22%	Grade 2 (moderate)
>22%	Grade 3 (severe)

Source.—Adapted and reprinted, with permission, from reference 43.

SWE techniques can also be used to evaluate the clinical outcome, including the risk of liver-related events, in patients with diffuse liver disease (59). One key feature of SWE is that with the continuous numerical values, the delta LS change over time is helpful in noninvasively evaluating progression or regression of a disease regardless of the cause (67), even in patients who do not have liver fibrosis but are affected by diseases that increase LS. Elastography gives an LS "value" that is just one marker of disease. It needs to be interpreted in the clinical context considering clinical and laboratory data, treatment, and other conditions. In children with CLD, SWE can be used to separate normal from abnormal results and serially monitor individuals over time during treatment (59,68). Since LS measurement reflects stiffness, not fibrosis, beyond liver fibrosis assessment, LS is a useful parameter for evaluating liver congestion that occurs in right-sided heart failure, congenital cardiac and valvular diseases, hepatic sinusoidal obstruction syndrome, and Budd-Chiari syndrome (67,69,70).

In patients with chronic hepatitis C infection successfully treated with direct-acting antivirals (DAAs), rapid LS decline has been reported by several studies related to resolution of inflammation rather than liver fibrosis improvement. The update to the SRU consensus proposed following patients treated with DAAs by using LS values obtained at the end of treatment as a baseline and to assess the clinical outcome by evaluating the LS delta change over time with respect to this baseline (59).

It should be noted that with US, LSM is reported as the Young modulus in kilopascals, while with MRE, LSM is reported as the magnitude of the complex shear modulus, also in kilopascals. US measurements in kilopascals are approximately three times the kilopascals reported with MRE when performed at the same frequency (58). However, since the Young modulus and shear modulus measure two different entities, conversion of LSM measurements obtained with US SWE and MRE should generally be avoided.

US SWE Artifacts, Tips, and Tricks

Recognizing and understanding artifacts is critical in performing and interpreting US SWE LS measurements. Several types of SWE LSM artifacts are very common. Artifacts can result from poor acquisition, tissue composition, and operator error. Artifacts can overestimate or underestimate LS values. It is important to realize that shear wave speed estimates are made from B-mode tracking pulses, so if the B-mode image is poor

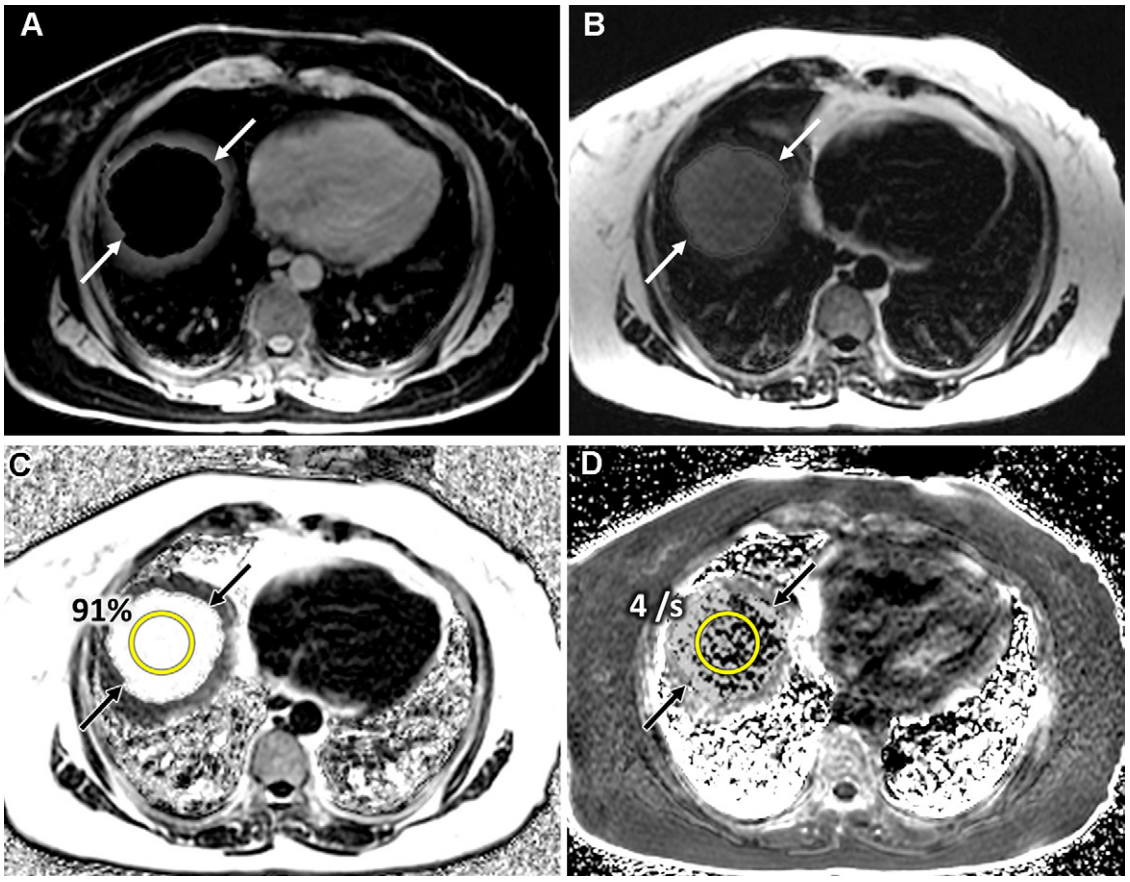

Figure 17. Local fat-water swap artifact on a water image **(A)**, fat image **(B)**, PDFF map **(C)**, and R2* map **(D)**. In rare cases, the chemical shift–encoded reconstruction can have either local **(A–D)** or rarely global (Fig 18) swapping of the fat and water signals. In the region of the swaps (arrows), the PDFF value can be nonsensical, showing 91% in the liver on **C**, which is incorrect. Although R2* values may or may not be sensible **(D)**, these values are also incorrect, as PDFF and R2* are estimated simultaneously, and the accuracy of one map depends on the accuracy of the other map. *s* = second.

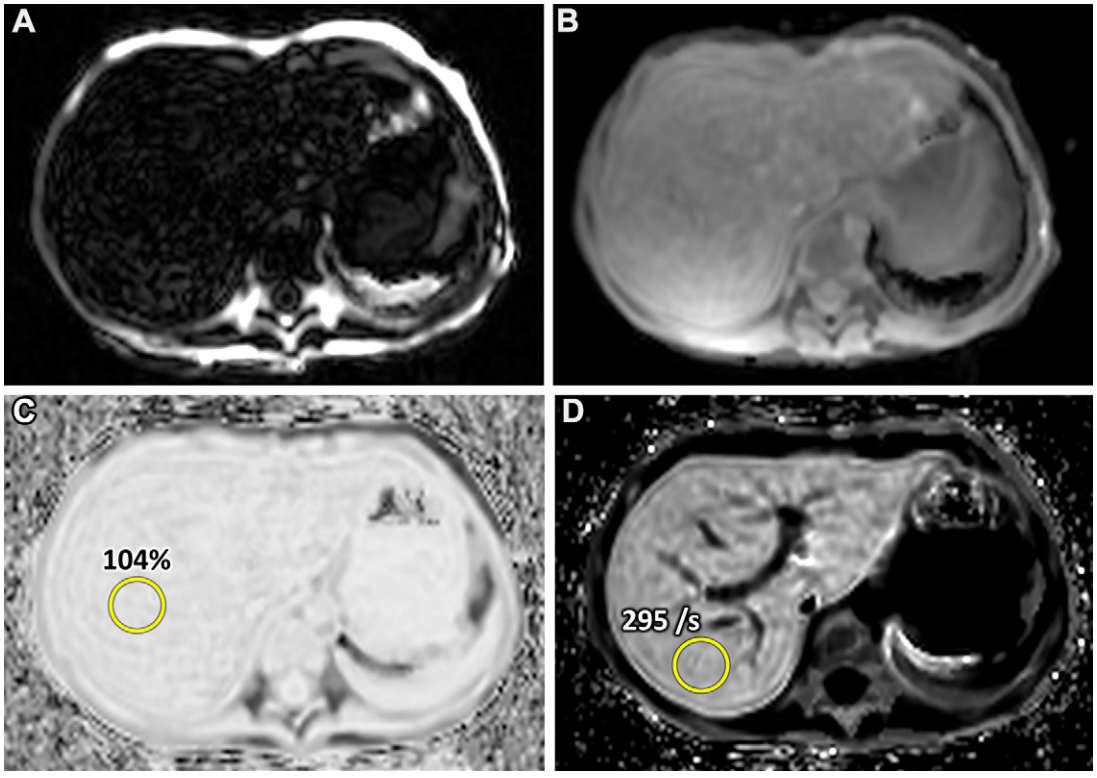

Figure 18. Global fat-water swap artifact on a water image **(A)**, fat image **(B)**, PDFF map **(C)**, and R2* map **(D)**. In some cases, the chemical shift–encoded reconstruction can have either a local (Fig 17) or rarely global **(A–D)** swapping of the fat and water signals. In the region of the swaps, the PDFF value can be nonsensical, showing 104% PDFF in the liver on **C**, which is incorrect. Although R2* values may or may not be sensible **(D)**, these values are also incorrect, as PDFF and R2* are estimated simultaneously, and the accuracy of one map depends on the accuracy of the other map. In cases of global fat-water swaps, adjusting the shim-box and reshimming and/or shortening the initial TE or interecho interval may be helpful. *s* = second.

or has artifacts, LS estimates will be inaccurate. Following a standard protocol when acquiring measurements can decrease artifacts resulting from operator technique.

In most 2D SWE products, a quality map/factor is available that is helpful for identifying and avoiding artifacts. However, with pSWE, this tool is not available, and it is

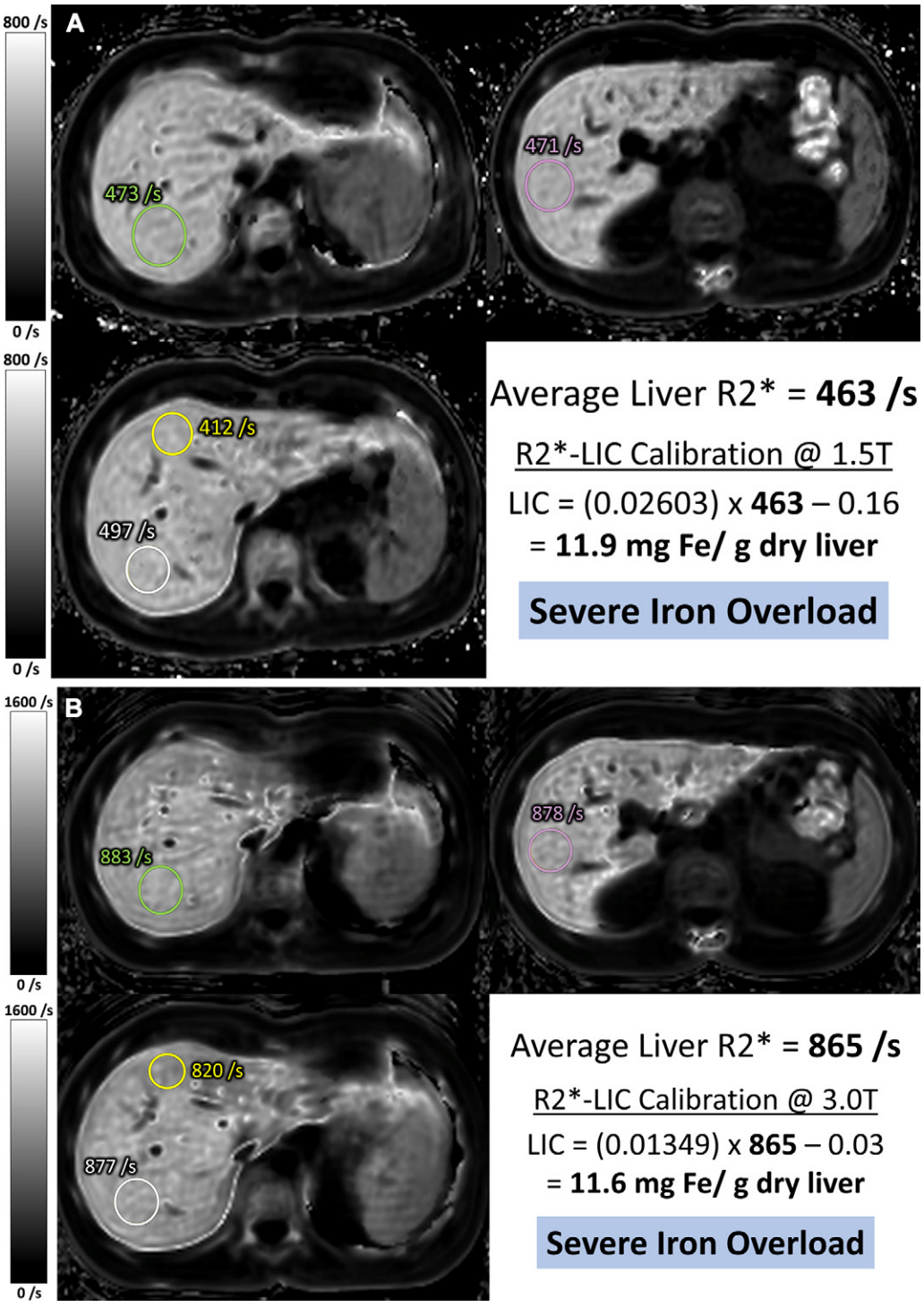

Figure 19. Examples of ROI placement on R2* maps. Similar to PDFF maps, at least four circular ROIs with a diameter of 2 cm or greater should be drawn, at least two in the right lobe and at least one in the left lobe. The average R2* value of the four or more ROIs is used to estimate the LIC by using a field strength–specific calibration formula (Table 5). **A** shows an R2* map and four ROIs at 1.5 T in a patient with severe iron overload. **B** shows the R2* map and ROIs at 3 T in the same patient. By using the appropriate field strength–specific calibration formula, LIC can be estimated by using 1.5-T or 3-T MRI. *s* = second.

therefore important to carefully place the measurement box away from areas known to create artifacts (eg, liver capsule, blood vessels, areas of shadowing). Table S2 lists artifacts that are common in US SWE LS measurements and describes how to detect and avoid them (Figs 23A, 24B, 27–29). Table S3 provides tips and tricks for US SWE LS measurement.

US Fat Quantification

Overview

Conventional B-mode US is widely used to qualitatively assess liver steatosis (71). It has been reported to have a 100% sensitivity and 90% specificity to detect steatosis in 20% or more of

Table 5: Magnetic Field Strength Specific LIC Calibration Equations

Field Strength	Vendor(s)	Equation
1.5 T	General Electric, Philips, Siemens	LIC = 0.02603 × R2* – 0.16
3.0 T	General Electric, Philips	LIC = 0.01349 × R2* – 0.03
2.89 T	Siemens*	LIC = 0.01400 × R2* – 0.03

Source.—Adapted and reprinted, with permission, from reference 51.
*Siemens 3-T systems operate at a nominally lower field strength; since the susceptibility effect scales with the field strength, a Siemens-specific calibration curve is provided for their 3-T systems.

Table 6: R2* and LIC Values Corresponding to Subjective Severity Indices of Iron Overload

LIC (mg Fe/g dry liver)	R2* at 1.5 T (per second)	R2* at 3.0 T (per second)	R2* at 2.89 T (per second)	Iron Overload Subjective Severity
<1.8	<75	<136	<131	None (normal)
1.8–3.2	75–128	136–238	131–230	Mild
3.2–7.0	129–274	239–520	231–501	Moderate
7.0–15.0	275–581	521–1113	502–1073	Severe
≥15.0	≥582	≥1114	≥1074	Extreme

Source—Adapted and reprinted, with permission, from references 46 and 51.

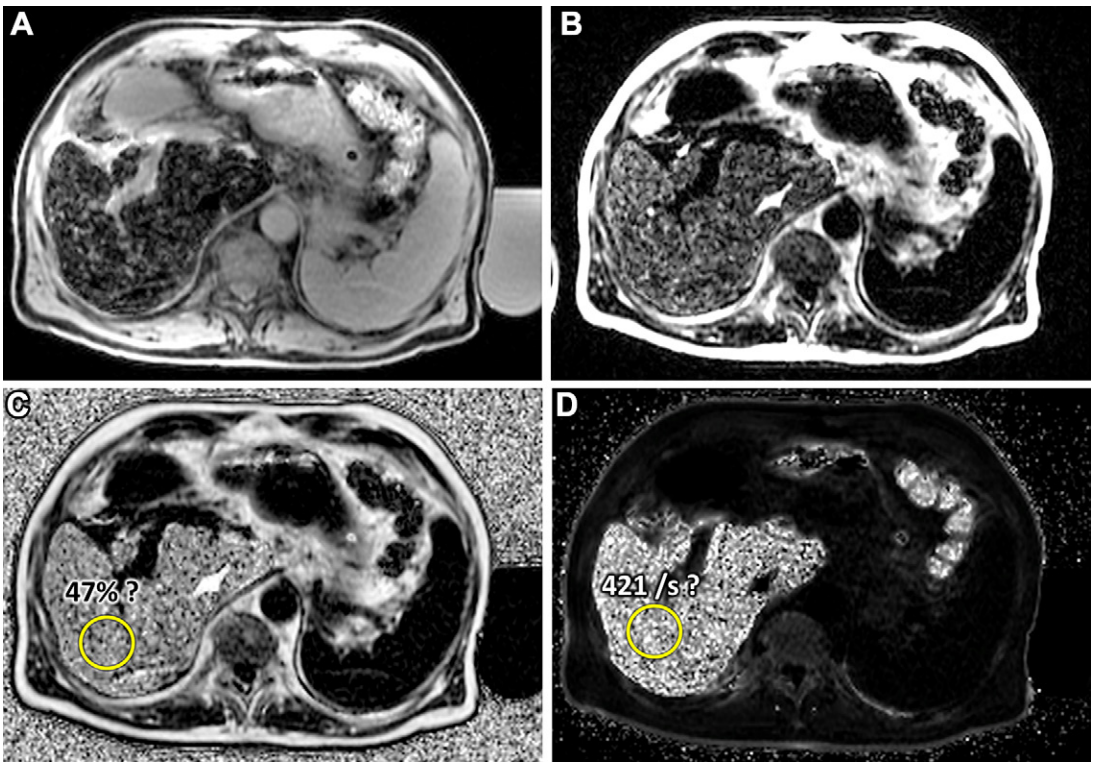

Figure 20. PDFF and R2* estimation failure due to severe iron overload as demonstrated on a water image **(A)**, fat image **(B)**, PDFF map **(C)**, and R2* map **(D)**. In severely iron-loaded livers, signal loss in the liver over the multiple TEs may be too rapid for reliable R2* estimation. In these cases, the nominal R2* estimates can have large variability, and the map becomes speckled or pixelated **(D)**. This appearance is not biologically plausible, as iron deposition is locally homogeneous. Because all reconstructed images of the chemical shift–encoded sequence are interdependent, failure of reliable R2* estimation is similarly translated to failure to reliably estimate the PDFF map **(C)**, as well as the water and fat images **(A, B)**. These poor fitting artifacts can be partially overcome by using the shortest achievable initial TE and interecho interval (both <1 msec) but may remain problematic at very high liver iron concentrations. *s* = second.

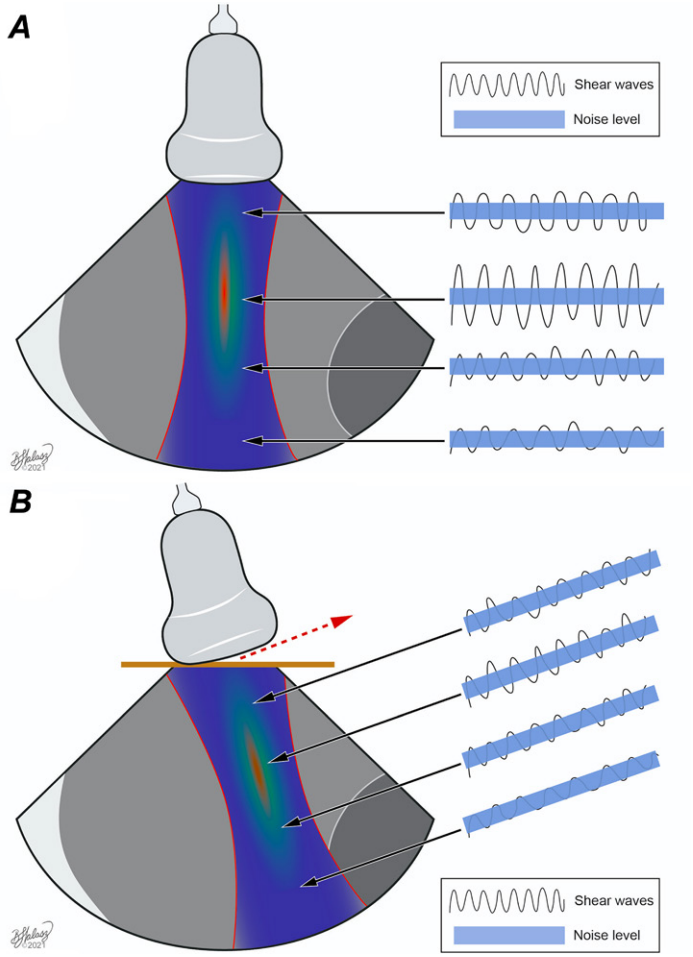

Figure 21. Illustrations show the effect on the shear wave amplitude when the transducer is perpendicular to (as in *A*), and not perpendicular to (as in *B*) the liver capsule. Note that the shear waves have higher amplitude when the transducer is perpendicular to the liver capsule. When the transducer is angled to the liver capsule, the shear wave amplitude is decreased because of refraction of energy (dotted red arrow) weakening the ARFI pulse. This leads to inaccurate measurement of LS. (Reprinted, with permission, from Beth A. Halasz, Copyright © 2022.)

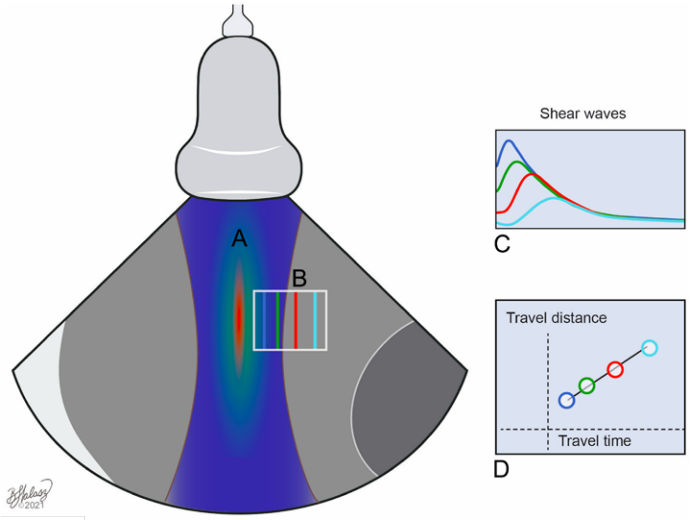

Figure 22. Illustration demonstrates the criteria used to evaluate the quality of the shear wave velocity assessment. *A* is the strength of the ARFI pulse, with red indicating more energy deposition. *B* is the location of the B-mode tracking pulses. Most quality maps evaluate the quality of the shear waves by assessing the height of the shear waves, signal-to-noise ratio of the shear waves, and whether the displacement curves, *C,* follow a regular pattern and if the slope of the distance from the ARFI pulse to the time of the maximum displacement curve peak is a straight line, *D*. The combination of the quality of each of these factors is summarized into one number, usually from 0 (no confidence) to 100 (high confidence). (Reprinted, with permission, from Beth A. Halasz, Copyright © 2022.)

hepatocytes but is less sensitive for detecting lower degrees of liver fat (72). Subjective assessment of gray-scale US is limited by substantial interobserver variability. To improve liver fat quantification with B-mode US, the hepatorenal index (HRI) has been developed (73). This method compares the echo intensity of the liver parenchyma to that of the renal cortex, assuming a normal kidney. The HRI is impacted by operator experience, measurement depth, and vendor algorithm variability for calculating measurements. The literature has significant variability, with the HRI optimal cutoff ranging from 1.24 to 2.2 for diagnosing steatosis (74). To improve measurement accuracy, vendors have used raw data to account for the time-gain compensation curve (74,75).

New quantitative US methods to assess liver fat content have recently been developed (76). These techniques analyze the radiofrequency echoes returning to the transducer and calculate parameters that can be used to quantify liver fat content. They include attenuation coefficient, backscatter coefficient, and speed of sound, as well as combinations of these (Figs 30, S7; Appendix S1). Controlled attenuation parameter (CAP) (ie, the attenuation coefficient on the FibroScan system) is not discussed in this article. However, it must be highlighted that CAP must not be used as a reference standard in studies that assess the performance of new fat quantification algorithms due to its suboptimal performance in detecting and grading liver fat content (77,78).

At the time of this article, there are several articles on the use of the attenuation coefficient and some articles on the combination of attenuation and backscatter suggesting that these techniques have good agreement with MRI PDFF (77,78). In fact, one vendor combined attenuation and backscatter coefficients to create a "US-derived fat fraction" that is reported as a percentage that seems highly correlative with MRI PDFF (79). However, further studies are needed to better specify how to perform these examinations and better define cutoff values. Backscatter and speed of sound techniques have limited discussion in the literature, and further studies are needed to define their role in US liver fat quantification. Regarding reporting results, for all US techniques, it is currently recommended to report fat quantification based on the vendor's recommended cutoff values (78).

Attenuation.—US attenuation-based fat quantification techniques rely on energy loss of the acoustic signals while traveling through tissue. The presence of fat in tissue increases the attenuation and thus the signal delay. However, attenuation is also dependent on the ultrasound frequency used. It is possible to quantify this energy loss while taking frequency into account and thus quantify tissue fat content.

The attenuation estimation techniques have been validated using a phantom with known attenuation values and

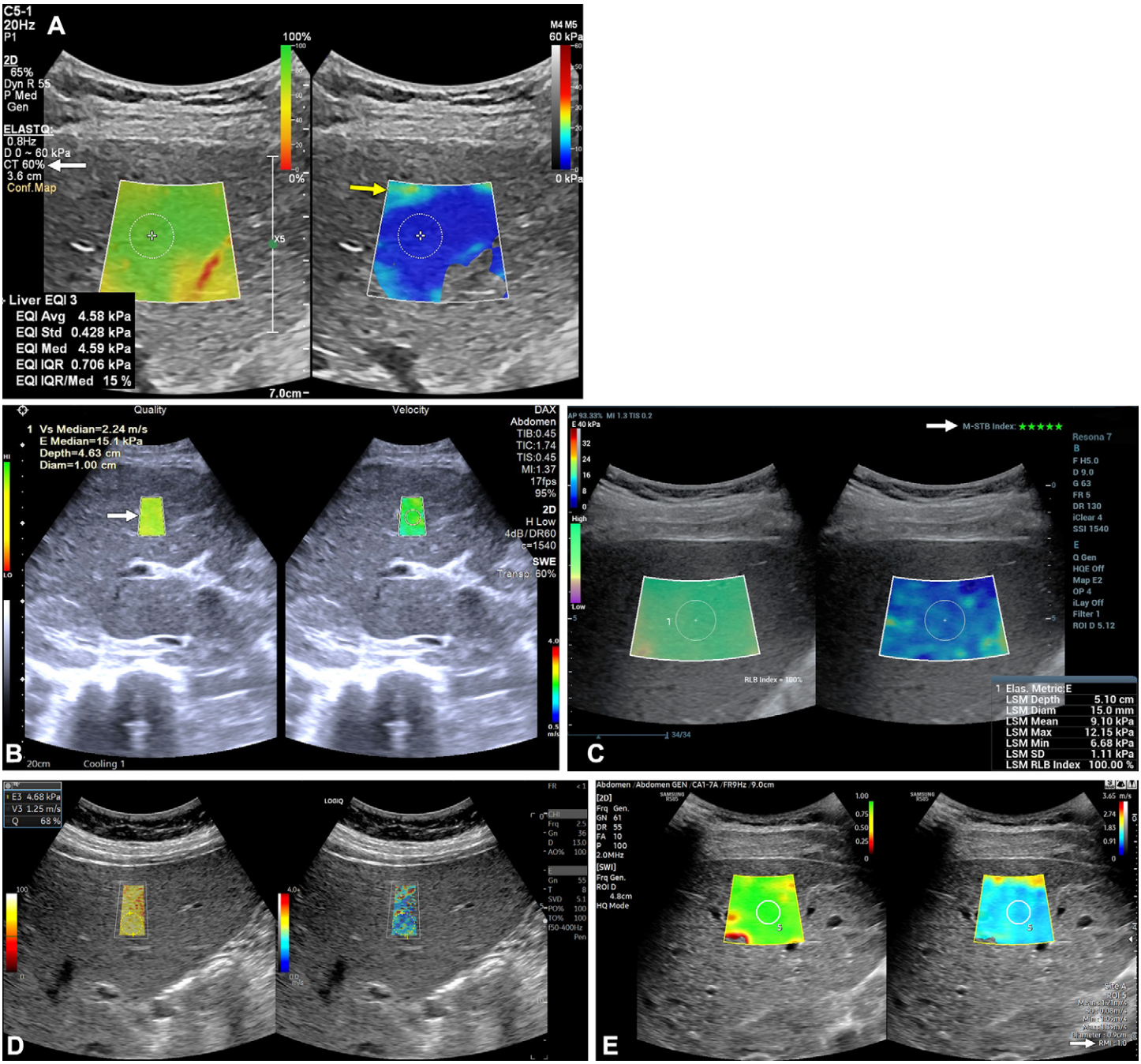

Figure 23. Manufacturer quality criteria for 2D SWE techniques: color-coded quality map. 2D SWE images obtained on US systems from five different manufacturers (in five different patients) show the color-coded quality maps (left images) and elasticity maps (right images). Generally on the quality maps, the highest quality is in green, whereas red indicates very poor quality. **(A)** In this case, the user can set a "confidence threshold" *(CT)* (white arrow). At 60%, as in this case, the low- and some medium-quality signals are filtered out in the elasticity map. There is reverberation artifact due to the liver capsule in the near field (yellow arrow). **(B)** In this case, the areas colored in green or yellow are of acceptable quality (arrow). **(C)** In this case, the color of the quality map *(RLB)* goes from purple, indicating poor reliability, to green, indicating the highest reliability. Another quality criterion of this vendor is the motion stability *(M-STB)* index (arrow) indicated by stars: the highest stability is indicated by five green stars, whereas red stars indicate motion. **(D)** In this case, the quality map ranges from zero (no confidence, red) to 100 (high confidence, white). The contour of the measurement box is white (as depicted here) if the software judges the measurement of high quality; otherwise it is in red color. **(E)** In this case, the quality of each measurement (circle) is assessed with a reliability measurement index *(RMI)* (arrow).

mathematical simulations. Factors affecting the accuracy of attenuation estimation include backscattering variation, speed of sound variation, focus location, imaging artifacts, imaging resolution, and signal-to-noise ratio. The sizes of the ROIs and analysis window are often optimized based on these factors in implementing an attenuation estimation technique (80). The depth of the ROI can be limited by the signal-to-noise ratio level. All vendor algorithms are designed to exclude large blood vessels and artifacts in the ROI from measurements, which may increase the method's accuracy (77,78). Attenuation results are provided in decibels per centimeter per megahertz and should be reported to the nearest second decimal (eg, ATI 0.62 dB/cm/MHz, not 0.621 dB/cm/MHz).

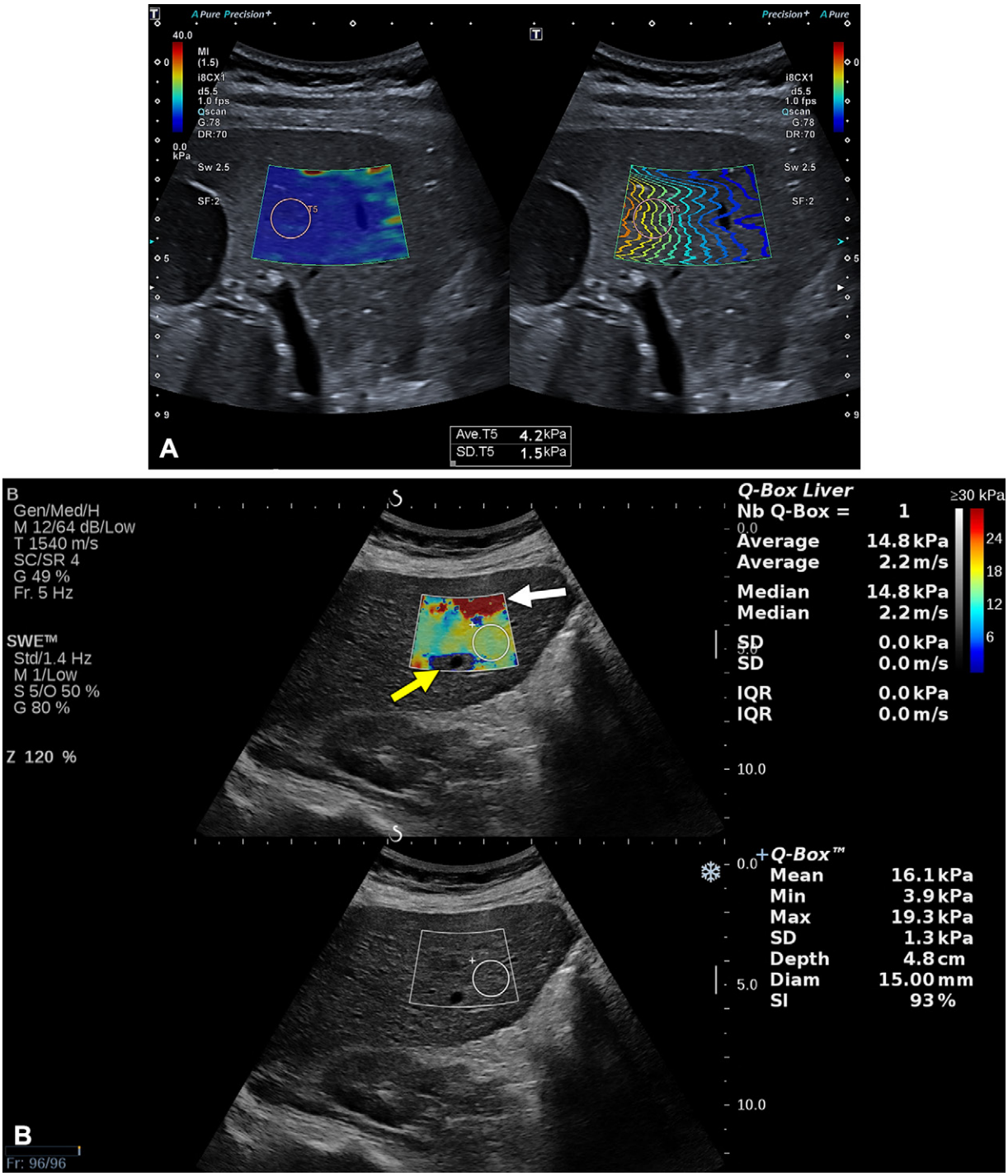

Figure 24. Manufacturer quality criteria for 2D SWE techniques: propagation map and stability index. 2D SWE images were obtained on US systems from two different manufacturers in two different patients. **(A)** The propagation map (right image), which is a quality assessment map, and the elasticity map (left image) are shown side by side. A good acquisition has a propagation map with parallel lines, and the intervals between the lines have the same distance. The propagation map is the guidance for placing the measurement box (circles). **(B)** Stability index *(SI)* (bottom image) is an indicator of temporal stability and is displayed while positioning the measurement box. The software filters out values with a low signal-to-noise ratio, and these areas are left blank. An acquisition of good quality should have an SI greater than 90%. There is reverberation artifact in the near field (white arrow) and a blank area around the vessel in the far field (yellow arrow).

Backscatter.—Another quantitative US technique is the use of backscattered signals from tissue to detect intrahepatocyte fat. Fat vacuoles within hepatocytes increase ultrasound scattering signals, resulting in greater backscatter and a brighter liver appearance (ie, more echogenic) (77).

Speed of Sound.—Speed of sound measurement is another US biomarker of hepatic steatosis. Speed of sound decreases proportionally to increased liver fat content. Limitations include potential confounding factors such as inflammation, parenchymal edema, increased intracapsular pressure, and

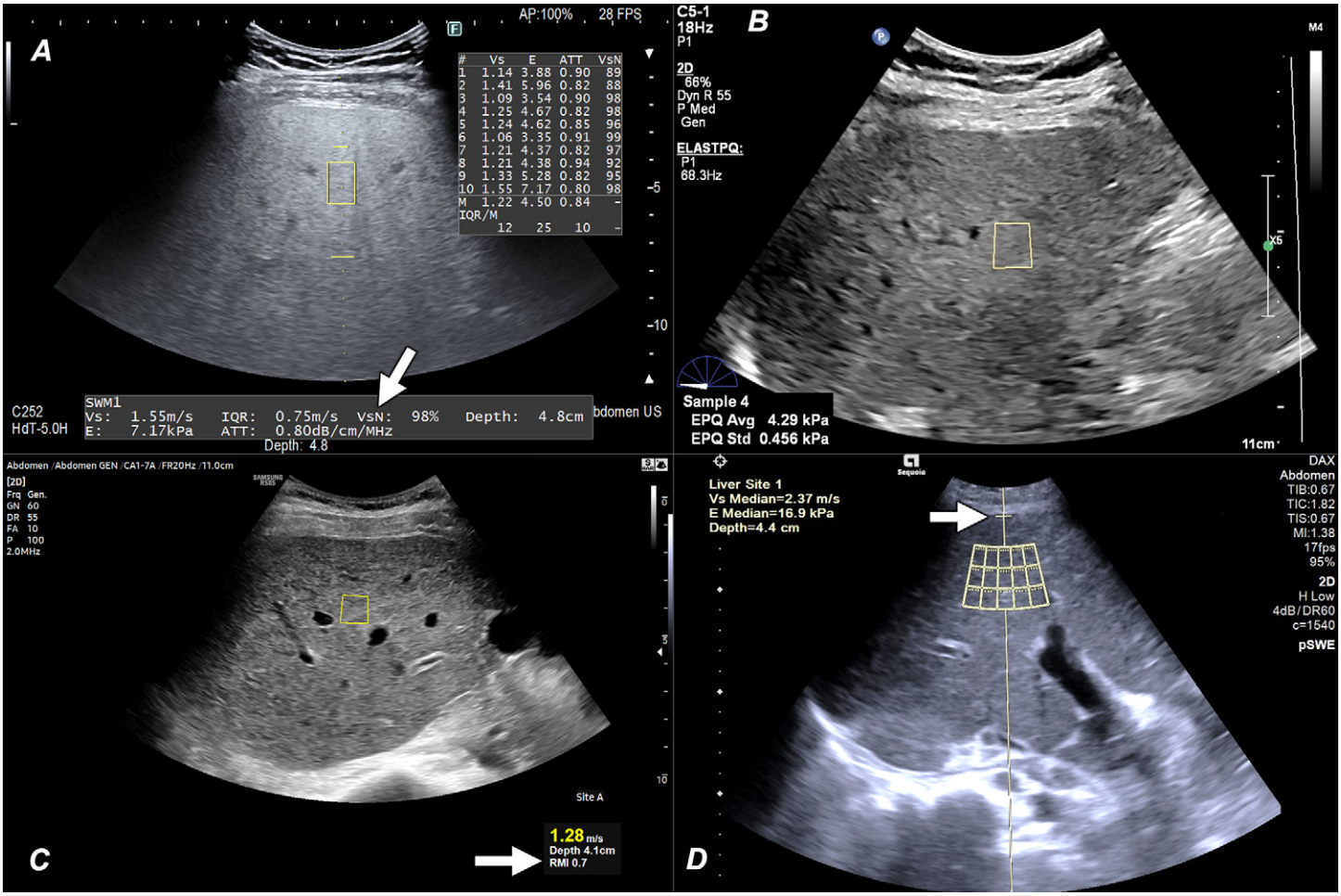

Figures 25. Manufacturer quality criteria for point SWE (pSWE) techniques. pSWE images, *A–D*, obtained with four US systems from different manufacturers (in four different patients). *A,* VsN (arrow) is a reliability index that indicates the percentage of effective push-track sequences. A measurement of good quality should have a VsN greater than or equal to 50%. When the signal-to-noise ratio of an acquisition is very low, the mean value is not shown. *B,* The mean value of the push-track sequences is given together with the standard deviation (SD). An SD less than or equal to 30% of the mean value indicates an acquisition of good quality. When the signal-to-noise ratio of an acquisition is very low, the mean value is not shown. *C,* The quality of each measurement is assessed with a reliability measurement index *(RMI)* (arrow). *D,* This system takes 15 pSWE measurements with a single button push, evaluates the quality of the shear waves (shown with dots in each small rectangle), and deletes the measurements felt to be unreliable. The horizontal line above the measurement area (arrow) is placed at the liver capsule to standardize the measurement depth. The deep abdominal transducer *(DAX)* used for this software has a lower frequency allowing deeper penetration. It is calibrated to provide similar stiffness measurements to the standard C5 transducer, although the frequency is lower, to allow measurements of LS up to 14 cm.

Table 7: Recommendations for Interpretation of LS Values Obtained with ARFI Techniques in Patients with Viral Hepatitis and Nonalcoholic Fatty Liver Disease (Rule of Four)

LS Value	Recommendation
≤5 kPa (1.3 m/sec)	High probability of being normal
<9 kPa (1.7 m/sec)	In the absence of other known clinical signs, rules out cACLD; if there are known clinical signs, may need further test for confirmation
9–13 kPa (1.7–2.1 m/sec)	Suggestive of cACLD but need further test for confirmation
>13 kPa (2.1 m/sec)	Rules in c ACLD
>17 kPa (2.4 m/sec)	Suggestive of CSPH

Source.—Adapted and reprinted, with permission, from reference 59.
Note.—CSPH = clinically significant portal hypertension.

Liver stiffness measurements were obtained on a (list vendor and machine) using a (list probe) following the SRU guidelines. (# number of) valid measurements were obtained using a (point-SWE or 2D-SWE) method. The IQR-to-median ratio was (x) suggesting a (quality data set or poor-quality data set). The liver stiffness value was (X) suggesting **(rule of 4 recommended wording)**. Consider adding the following sentence(s) if appropriate: In the setting of (elevated liver function tests, non-fasting, vascular congestion, etc.), the stage of liver fibrosis may be overestimated; In some patients with NAFLD, the cut-off values for cACLD may be lower (7–9 kPa); In etiologies other than viral hepatitis and NAFLD, the cut-off values are not well established.

Figure 26. Suggested dictation template macro for ARFI technique. *IQR* = interquartile range, *NAFLD* = nonalcoholic fatty liver disease, *SRU* = Society of Radiologists in Ultrasound, *2D* = two-dimensional. (Adapted, with permission, from reference 59.)

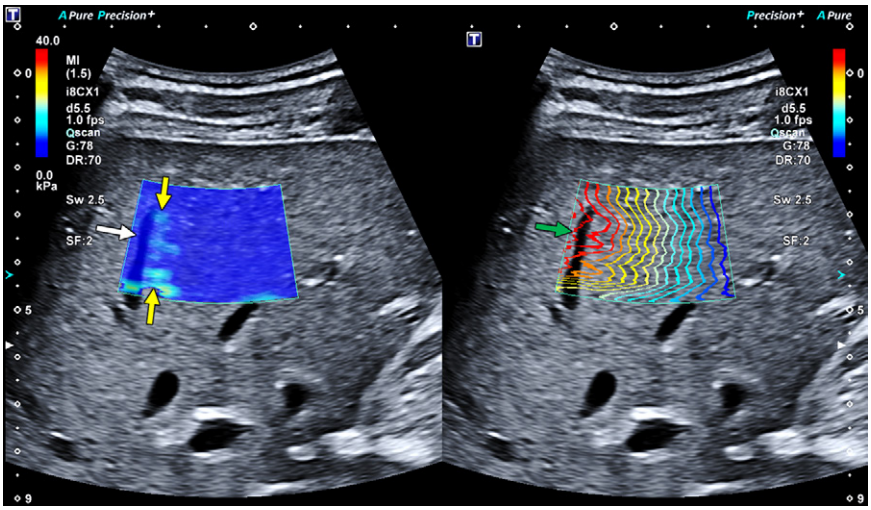

Figure 27. Artifact due to vessel pulsation. 2D SWE elasticity map (left) shows a vessel that is included in the field of view (white arrow). The elasticity map shows an increase in stiffness around the vessel (yellow arrows). The lines on the propagation map (right) are spread apart and not parallel, indicating low quality (green arrow).

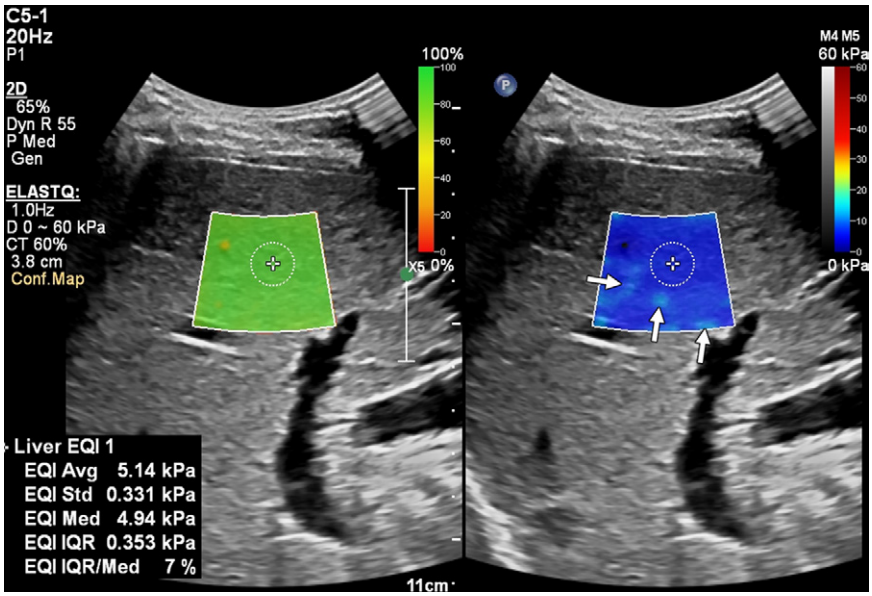

Figure 28. Artifacts from blood vessels just out of the image plane. 2D SWE images show a quality map (left) and elasticity map (right). Shear-wave propagation occurs in all directions perpendicular to the push pulse of the ultrasound beam. In the elasticity map (right), these blood vessel artifacts can be seen as teal (ie, blue-green) areas (arrows). The measurement box should not include these areas. Note that the quality map (left) suggests high-quality signals throughout the field of view. The quality map does not identify all artifacts, and for this reason, both the quality map and the elasticity map should be evaluated to detect artifacts.

temperature change, as higher temperatures increase speed of sound values and vice versa (77).

Conclusion

Quantifying liver fibrosis, fat, and iron with MRI and fibrosis and fat with US are important clinical tools in evaluating patients with CLD, replacing liver biopsy in most patient care settings. This article provides a primer for using MRI and US to evaluate these key imaging biomarkers. Our goal is to provide a helpful guide for practicing physicians and trainees interpreting these studies.

Author affiliations.—From the Department of Radiology, Thomas Jefferson University, 132 S 10th St, Philadelphia, PA 19107 (F.F.G.); Department of Radiology, Northeastern Ohio Medical University, Rootstown, Ohio (R.G.B.); Department of Radiology and Advanced Imaging Research Center, University of Texas Southwestern Medical Center, Dallas, Tex (T.Y.); Department of Clinical, Surgical, Diagnostic and Pediatric Sciences, University of Pavia, Pavia, Italy (G.F.); Department of Radiology, University of Kentucky, Lexington, Ky (J.T.L.); Department of Radiology, Cincinnati Children's Hospital Medical Center, University of Cincinnati College of Medicine, Cincinnati, Ohio (J.R.D.); Department of Radiology, Northwestern University Feinberg School of Medicine, Chicago, Ill (J.M.H., F.H.M.); Joint Department of Medical Imaging, University Health Network, University of Toronto, Toronto, Ontario, Canada (K.S.J.); Department of Radiology, ChristianaCare, Newark, Del (R.Y.M.); Department of Radiology, Massachusetts General Hospital,

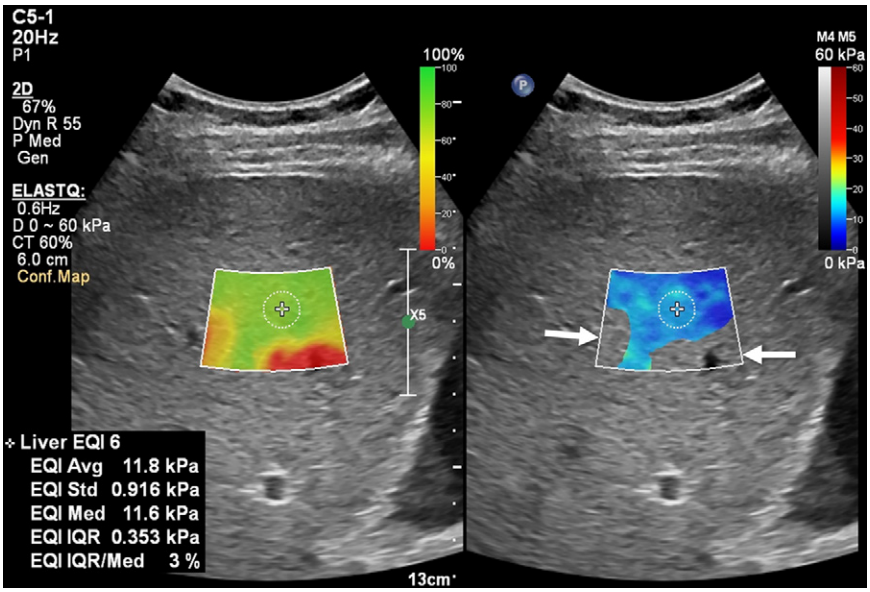

Figure 29. Signal dropout resulting from limited penetration. 2D SWE images show a quality map (left) and elasticity map (right). The maximum strength of the push-pulse of the ultrasound beam is at 4–4.5 cm from the transducer. In this case, the field of view was positioned too deep, and the far part of the field of view is 7 cm from the transducer. At this depth, the strength of the push-pulse is attenuated, leading to low signal-to-noise ratio in the estimate of tissue stiffness. For this reason, part of the elasticity map is void of color (arrows).

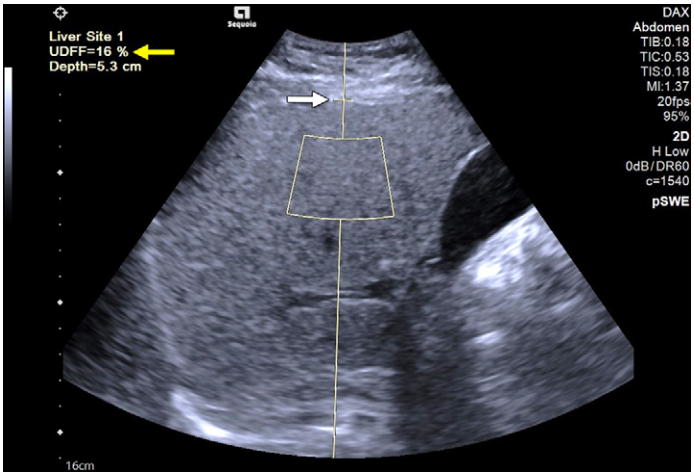

Figure 30. Attenuation coefficient and backscatter coefficient combined. With this US system, a value is given as a US-derived fat fraction (*UDFF*, yellow arrow), which is the percentage of liver fat content. The horizontal line above the measurement box (white arrow) is used to standardize the depth of measurement and should be placed at the level of the liver capsule.

Harvard Medical School, Boston, Mass (A.M.); Department of Radiology and Biomedical Imaging, University of California, San Francisco, San Francisco, Calif (M.A.O., B.M.Y.); Departments of Radiology and Medical Physics (A.P.) and Departments of Radiology, Medical Physics, Biomedical Engineering, Medicine, and Emergency Medicine (S.B.R.), University of Wisconsin, Madison, Wis; Department of Radiology, NYU Langone Health, New York, NY (K.S.); Department of Radiology, Mayo Clinic, Phoenix, Ariz (A.C.S.); Department of Radiology, University of Alabama at Birmingham, Birmingham, Ala (E.N.S.); Department of Radiology, University of Texas MD Anderson Cancer Center, Houston, Tex (V.R.S.); Department of Diagnostic, Molecular and Interventional Radiology, BioMedical Engineering and Imaging Institute, Icahn School of Medicine at Mount Sinai, New York, NY (B.T.); and Department of Radiology, Mayo Clinic, Rochester, Minn (C.L.W., S.K.V.). Received August 7, 2022; revision requested September 16 and received October 10; accepted October 11. **Address correspondence to** F.F.G. (email: *flavius.guglielmo@jefferson.edu*).

***Disclosures of conflicts of interest.*—R.G.B.** Equipment and research grants from Philips Ultrasound, Siemens Ultrasound, Mindray Ultrasound, Samsung Ultrasound, and Hologic Ultrasound; royalties from Thieme and Elsevier; payment for lectures from Philips Ultrasound, Siemens Ultrasound, Canon Ultrasound, Canon MRI, Mindray, Bracco Diagnostics, Samsung Ultrasound; editor-in-chief of the *Journal of Ultrasound in Medicine*; member of QIBA; treasurer of the International Contrast Ultrasound Society. **T.Y.** Research grant from Siemens Healthineers. **G.F.** Honoraria for lectures from Canon Medical Systems, Fujifilm Medical Systems, Siemens Healthineers; support for attending meetings and/or travel from Fujifilm Medical Systems, speaker for Philips Medical Systems; royalties from Elsevier; member of QIBA. **J.R.D.** Grants from Philips Healthcare, GE Healthcare, Perspectum, Motilent, Bracco. **K.S.J.** Grants from Bayer and GE Healthcare. **F.M.** Consultant for Bayer Health Care and Guerbet Medical Advisory Board; member of QIBA. **A.P.** Consultancy fees from Sanofi Genzyme, Otsuka; research support to the University of Wisconsin from GE Healthcare and Bracco Diagnostics (unrelated to the current work). **S.B.R.** Ownership interests in Calimetrix, Reveal Pharmaceuticals, Cellectar Biosciences, Elucent Medical, HeartVista, and RevOps (unrelated to the current work); research support to the University of Wisconsin from GE Healthcare and Bracco Diagnostics (unrelated to the current work). **B.T.** Research support from Bayer, Takeda, Regeneron, Guerbet, Helio Health, Echosens, and Siemens; consultant for Bayer, Guerbet, and Ascelia. **B.M.Y.** Grants from and consultant and speaker for GE and Philips Medical Systems; founder of, shareholder in, member of the Board of Directors of Nextrast; consultant and speaker for Canon Medical; royalties from UCSF and Oxford University Press. **S.K.V.** Patent for system and method for generating nonalcoholic fatty liver disease activity score using MR elastography (licensee, Mayo Foundation for Medical Education and Research).

References

1. Moon AM, Singal AG, Tapper EB. Contemporary epidemiology of chronic liver disease and cirrhosis. Clin Gastroenterol Hepatol 2020;18(12):2650–2666.
2. Younossi ZM, Stepanova M, Younossi Y, et al. Epidemiology of chronic liver diseases in the USA in the past three decades. Gut 2020;69(3):564–568.
3. Cadranel JF, Rufat P, Degos F. Practices of liver biopsy in France: results of a prospective nationwide survey. For the Group of Epidemiology of the French Association for the Study of the Liver (AFEF). Hepatology 2000;32(3):477–481.
4. Horowitz JM, Venkatesh SK, Ehman RL, et al. Evaluation of hepatic fibrosis: a review from the society of abdominal radiology disease focus panel. Abdom Radiol (NY) 2017;42(8):2037–2053.
5. Kinner S, Reeder SB, Yokoo T. Quantitative imaging biomarkers of NAFLD. Dig Dis Sci 2016;61(5):1337–1347.
6. Pepin KM, Welle CL, Guglielmo FF, Dillman JR, Venkatesh SK. Magnetic resonance elastography of the liver: everything you need to know to get started. Abdom Radiol (NY) 2022;47(1):94–114.
7. Guglielmo FF, Venkatesh SK, Mitchell DG. Liver MR elastography technique and image interpretation: pearls and pitfalls. RadioGraphics 2019;39(7):1983–2002.
8. QIBA MR Biomarker Committee. MR Elastography of the Liver, Quantitative Imaging Biomarkers Alliance. Profile Stage: Technically Confirmed. https://qibawiki.rsna.org/index.php/Profiles. Published 2022. Updated February 14, 2022.

9. Venkatesh SK, Ehman RL. Magnetic resonance elastography of liver. Magn Reson Imaging Clin N Am 2014;22(3):433–446.
10. Venkatesh SK, Yin M, Ehman RL. Magnetic resonance elastography of liver: technique, analysis, and clinical applications. J Magn Reson Imaging 2013;37(3):544–555.
11. Wagner M, Corcuera-Solano I, Lo G, et al. Technical failure of MR elastography examinations of the liver: experience from a large single-center study. Radiology 2017;284(2):401–412.
12. Dzyubak B, Venkatesh SK, Manduca A, Glaser KJ, Ehman RL. Automated liver elasticity calculation for MR elastography. J Magn Reson Imaging 2016;43(5):1055–1063.
13. Srinivasa Babu A, Wells ML, Teytelboym OM, et al. Elastography in chronic liver disease: modalities, techniques, limitations, and future directions. RadioGraphics 2016;36(7):1987–2006.
14. Ichikawa S, Motosugi U, Nakazawa T, et al. Hepatitis activity should be considered a confounder of liver stiffness measured with MR elastography. J Magn Reson Imaging 2015;41(5):1203–1208.
15. Shi Y, Guo Q, Xia F, et al. MR elastography for the assessment of hepatic fibrosis in patients with chronic hepatitis B infection: does histologic necroinflammation influence the measurement of hepatic stiffness? Radiology 2014;273(1):88–98.
16. Wells ML, Fenstad ER, Poterucha JT, et al. Imaging findings of congestive hepatopathy. RadioGraphics 2016;36(4):1024–1037.
17. Kim DK, Choi JY, Park MS, Kim MJ, Chung YE. Clinical Feasibility of MR Elastography in Patients With Biliary Obstruction. AJR Am J Roentgenol 2018;210(6):1273–1278.
18. Hines CD, Lindstrom MJ, Varma AK, Reeder SB. Effects of postprandial state and mesenteric blood flow on the repeatability of MR elastography in asymptomatic subjects. J Magn Reson Imaging 2011;33(1):239–244.
19. Yin M, Talwalkar JA, Glaser KJ, et al. Dynamic postprandial hepatic stiffness augmentation assessed with MR elastography in patients with chronic liver disease. AJR Am J Roentgenol 2011;197(1):64–70.
20. Mederacke I, Wursthorn K, Kirschner J, et al. Food intake increases liver stiffness in patients with chronic or resolved hepatitis C virus infection. Liver Int 2009;29(10):1500–1506.
21. Jhaveri KS, Hosseini-Nik H, Sadoughi N, et al. The development and validation of magnetic resonance elastography for fibrosis staging in primary sclerosing cholangitis. Eur Radiol 2019;29(2):1039–1047.
22. Chalasani N, Younossi Z, Lavine JE, et al. The diagnosis and management of nonalcoholic fatty liver disease: Practice guidance from the American Association for the Study of Liver Diseases. Hepatology 2018;67(1):328–357.
23. European Association for the Study of the Liver (EASL); European Association for the Study of Diabetes (EASD); European Association for the Study of Obesity (EASO). EASL-EASD-EASO Clinical Practice Guidelines for the management of non-alcoholic fatty liver disease. J Hepatol 2016;64(6):1388–1402.
24. Reeder SB, Cruite I, Hamilton G, Sirlin CB. Quantitative assessment of liver fat with magnetic resonance imaging and spectroscopy. J Magn Reson Imaging 2011;34(4):729–749.
25. Wood JC. Guidelines for quantifying iron overload. Hematology Am Soc Hematol Educ Program 2014;2014(1):210–215.
26. Angelucci E, Barosi G, Camaschella C, et al. Italian Society of Hematology practice guidelines for the management of iron overload in thalassemia major and related disorders. Haematologica 2008;93(5):741–752.
27. Kowdley KV, Brown KE, Ahn J, Sundaram V. ACG Clinical Guideline: Hereditary Hemochromatosis. Am J Gastroenterol 2019;114(8):1202–1218 [Published correction appears in Am J Gastroenterol 2019;114(12):1927.].
28. Labranche R, Gilbert G, Cerny M, et al. Liver iron quantification with MR imaging: a primer for radiologists. RadioGraphics 2018;38(2):392–412.
29. Brunt EM. Pathology of nonalcoholic fatty liver disease. Nat Rev Gastroenterol Hepatol 2010;7(4):195–203.
30. Levene AP, Goldin RD. The epidemiology, pathogenesis and histopathology of fatty liver disease. Histopathology 2012;61(2):141–152.
31. Dixon WT. Simple proton spectroscopic imaging. Radiology 1984;153(1):189–194.
32. Ma J. Dixon techniques for water and fat imaging. J Magn Reson Imaging 2008;28(3):543–558.
33. Reeder SB, Hu HH, Sirlin CB. Proton density fat-fraction: a standardized MR-based biomarker of tissue fat concentration. J Magn Reson Imaging 2012;36(5):1011–1014.
34. Yu H, Shimakawa A, McKenzie CA, Brodsky E, Brittain JH, Reeder SB. Multiecho water-fat separation and simultaneous R2* estimation with multifrequency fat spectrum modeling. Magn Reson Med 2008;60(5):1122–1134.
35. Yokoo T, Serai SD, Pirasteh A, et al; RSNA-QIBA PDFF Biomarker Committee. Linearity, bias, and precision of hepatic proton density fat fraction measurements by using MR imaging: a meta-analysis. Radiology 2018;286(2):486–498.
36. Qu Y, Li M, Hamilton G, Zhang YN, Song B. Diagnostic accuracy of hepatic proton density fat fraction measured by magnetic resonance imaging for the evaluation of liver steatosis with histology as reference standard: a meta-analysis. Eur Radiol 2019;29(10):5180–5189.
37. Gu J, Liu S, Du S, et al. Diagnostic value of MRI-PDFF for hepatic steatosis in patients with non-alcoholic fatty liver disease: a meta-analysis. Eur Radiol 2019;29(7):3564–3573.
38. Armstrong T, Ly KV, Murthy S, et al. Free-breathing quantification of hepatic fat in healthy children and children with nonalcoholic fatty liver disease using a multi-echo 3-D stack-of-radial MRI technique. Pediatr Radiol 2018;48(7):941–953.
39. Armstrong T, Zhong X, Shih SF, et al. Free-breathing 3D stack-of-radial MRI quantification of liver fat and R_2* in adults with fatty liver disease. Magn Reson Imaging 2022;85:141–152.
40. Boyarko AC, Dillman JR, Tkach JA, Pednekar AS, Trout AT. Comparison of compressed SENSE and SENSE for quantitative liver MRI in children and young adults. Abdom Radiol (NY) 2021;46(10):4567–4575.
41. Lohöfer FK, Kaissis GA, Müller-Leisse C, et al. Acceleration of chemical shift encoding-based water fat MRI for liver proton density fat fraction and T2* mapping using compressed sensing. PLoS One 2019;14(11):e0224988.
42. Campo CA, Hernando D, Schubert T, Bookwalter CA, Pay AJV, Reeder SB. Standardized approach for ROI-based measurements of proton density fat fraction and R2* in the liver. AJR Am J Roentgenol 2017;209(3):592–603.
43. Tang A, Desai A, Hamilton G, et al. Accuracy of MR imaging-estimated proton density fat fraction for classification of dichotomized histologic steatosis grades in nonalcoholic fatty liver disease. Radiology 2015;274(2):416–425.
44. Pirasteh A, Yuan Q, Hernando D, Reeder SB, Pedrosa I, Yokoo T. Inter-method reproducibility of biexponential R_2 MR relaxometry for estimation of liver iron concentration. Magn Reson Med 2018;80(6):2691–2701.
45. St Pierre TG, El-Beshlawy A, Elalfy M, et al. Multicenter validation of spin-density projection-assisted R2-MRI for the noninvasive measurement of liver iron concentration. Magn Reson Med 2014;71(6):2215–2223.
46. St Pierre TG, Clark PR, Chua-anusorn W, et al. Noninvasive measurement and imaging of liver iron concentrations using proton magnetic resonance. Blood 2005;105(2):855–861.
47. Wood JC, Enriquez C, Ghugre N, et al. MRI R2 and R2* mapping accurately estimates hepatic iron concentration in transfusion-dependent thalassemia and sickle cell disease patients. Blood 2005;106(4):1460–1465.
48. Vasanawala SS, Yu H, Shimakawa A, Jeng M, Brittain JH. Estimation of liver T_2 in transfusion-related iron overload in patients with weighted least squares T_2 IDEAL. Magn Reson Med 2012;67(1):183–190.
49. Hernando D, Kramer JH, Reeder SB. Multipeak fat-corrected complex R2* relaxometry: theory, optimization, and clinical validation. Magn Reson Med 2013;70(5):1319–1331.
50. Ghugre NR, Wood JC. Relaxivity-iron calibration in hepatic iron overload: probing underlying biophysical mechanisms using a Monte Carlo model. Magn Reson Med 2011;65(3):837–847.
51. Hernando D, Zhao R, Yuan Q, et al. Multicenter Reproducibility of Liver Iron Quantification with 1.5-T and 3.0-T MRI. Radiology 2023 Feb;306(2):e213256
52. Hernando D, Cook RJ, Qazi N, Longhurst CA, Diamond CA, Reeder SB. Complex confounder-corrected R2* mapping for liver iron quantification with MRI. Eur Radiol 2021;31(1):264–275.
53. Jhaveri KS, Kannengiesser SAR, Ward R, Kuo K, Sussman MS. Prospective evaluation of an R2* method for assessing liver iron concentration (LIC) against FerriScan: derivation of the calibration curve and characterization of the nature and source of uncertainty in the relationship. J Magn Reson Imaging 2019;49(5):1467–1474.
54. d'Assignies G, Paisant A, Bardou-Jacquet E, et al. Non-invasive measurement of liver iron concentration using 3-Tesla magnetic resonance imaging: validation against biopsy. Eur Radiol 2018;28(5):2022–2030.
55. Henninger B, Zoller H, Rauch S, et al. R2* relaxometry for the quantification of hepatic iron overload: biopsy-based calibration and comparison with the literature. Rofo 2015;187(6):472–479.
56. Hankins JS, McCarville MB, Loeffler RB, et al. R2* magnetic resonance imaging of the liver in patients with iron overload. Blood 2009;113(20):4853–4855.
57. Shiina T, Nightingale KR, Palmeri ML, et al. WFUMB guidelines and recommendations for clinical use of ultrasound elastography: Part 1—basic principles and terminology. Ultrasound Med Biol 2015;41(5):1126–1147.
58. Barr RG, Ferraioli G, Palmeri ML, et al. Elastography Assessment of Liver Fibrosis: Society of Radiologists in Ultrasound Consensus Conference Statement. Radiology 2015;276(3):845–861.
59. Barr RG, Wilson SR, Rubens D, Garcia-Tsao G, Ferraioli G. Update to the Society of Radiologists in Ultrasound Liver Elastography Consensus Statement. Radiology 2020;296(2):263–274.
60. Ferraioli G, De Silvestri A, Lissandrin R, et al. Evaluation of Inter-System Variability in Liver Stiffness Measurements. Ultraschall Med 2019;40(1):64–75.

61. Gilligan LA, Trout AT, Bennett P, Dillman JR. Repeatability and agreement of shear wave speed measurements in phantoms and human livers across 6 ultrasound 2-dimensional shear wave elastography systems. Invest Radiol 2020;55(4):191–199.
62. Dietrich CF, Bamber J, Berzigotti A, et al. EFSUMB Guidelines and Recommendations on the Clinical Use of Liver Ultrasound Elastography, Update 2017 (Long Version). Ultraschall Med 2017;38(4):e16–e47 [Published correction appears in Ultraschall Med 2017;38(4):e48.].
63. Ferraioli G, Wong VW, Castera L, et al. Liver Ultrasound Elastography: An Update to the World Federation for Ultrasound in Medicine and Biology Guidelines and Recommendations. Ultrasound Med Biol 2018;44(12):2419–2440.
64. Ferraioli G, Barr RG. Interpreting liver stiffness values in clinical practice: Is the use of a histologic classification, correct? Radiology 2023; 307(1):e220553.
65. de Franchis R; Baveno VI Faculty. Expanding consensus in portal hypertension: Report of the Baveno VI Consensus Workshop: Stratifying risk and individualizing care for portal hypertension. J Hepatol 2015;63(3):743–752.
66. de Franchis R, Bosch J, Garcia-Tsao G, Reiberger T, Ripoll C; Baveno VII Faculty. Baveno VII - Renewing consensus in portal hypertension. J Hepatol 2022;76(4):959–974 [Published correction appears in J Hepatol 2022;77(1):271.].
67. Ferraioli G, Barr RG. Ultrasound liver elastography beyond liver fibrosis assessment. World J Gastroenterol 2020;26(24):3413–3420.
68. Ferraioli G, Barr RG, Dillman JR. Elastography for Pediatric Chronic Liver Disease: A Review and Expert Opinion. J Ultrasound Med 2021;40(5):909–928.
69. DiPaola FW, Schumacher KR, Goldberg CS, Friedland-Little J, Parameswaran A, Dillman JR. Effect of Fontan operation on liver stiffness in children with single ventricle physiology. Eur Radiol 2017;27(6):2434–2442.
70. Dohare N, Madhusudhan KS, Malik R, Das P, Sharma S. Utility of hepatic 2D shear-wave elastography in monitoring response to image-guided intervention in children with chronic Budd-Chiari syndrome: a prospective study. AJR Am J Roentgenol 2022;218(3):534–543.
71. Barr RG. Ultrasound of Diffuse Liver Disease Including Elastography. Radiol Clin North Am 2019;57(3):549–562.
72. Dasarathy S, Dasarathy J, Khiyami A, Joseph R, Lopez R, McCullough AJ. Validity of real time ultrasound in the diagnosis of hepatic steatosis: a prospective study. J Hepatol 2009;51(6):1061–1067.
73. Osawa H, Mori Y. Sonographic diagnosis of fatty liver using a histogram technique that compares liver and renal cortical echo amplitudes. J Clin Ultrasound 1996;24(1):25–29.
74. Chauhan A, Sultan LR, Furth EE, Jones LP, Khungar V, Sehgal CM. Diagnostic accuracy of hepatorenal index in the detection and grading of hepatic steatosis. J Clin Ultrasound 2016;44(9):580–586.
75. Ferraioli G, Soares Monteiro LB. Ultrasound-based techniques for the diagnosis of liver steatosis. World J Gastroenterol 2019;25(40):6053–6062.
76. Ozturk A, Grajo JR, Gee MS, et al. Quantitative Hepatic Fat Quantification in Non-alcoholic Fatty Liver Disease Using Ultrasound-Based Techniques: A Review of Literature and Their Diagnostic Performance. Ultrasound Med Biol 2018;44(12):2461–2475.
77. Ferraioli G, Berzigotti A, Barr RG, et al. Quantification of liver fat content with ultrasound: A WFUMB position paper. Ultrasound Med Biol 2021;47(10):2803–2820.
78. Ferraioli G, Kumar V, Ozturk A, Nam K, de Korte CL, Barr RG. US Attenuation for Liver Fat Quantification: An AIUM-RSNA QIBA Pulse-Echo Quantitative Ultrasound Initiative. Radiology 2022;302(3):495–506.
79. Dillman JR, Thapaliya S, Tkach JA, Trout AT. Quantification of Hepatic Steatosis by Ultrasound: Prospective Comparison With MRI Proton Density Fat Fraction as Reference Standard. AJR Am J Roentgenol 2022;219(5):784–791.
80. Nam K, Rosado-Mendez IM, Wirtzfeld LA, et al. Comparison of ultrasound attenuation and backscatter estimates in layered tissue-mimicking phantoms among three clinical scanners. Ultrason Imaging 2012;34(4):209–221.